Pore-scale investigation of colloid transport and retention in presence of dynamic air-water interface

Volha Lazouskaya,[1] Lian-Ping Wang,[2] Hui Gao,[2] Xiaoyan Shi,[2] Kirk Czymmek,[3] and Yan Jin[1]*

[1] Department of Plant and Soil Sciences, University of Delaware, Newark, DE 19716, USA

[2] Department of Mechanical Engineering, University of Delaware, Newark, DE 19716, USA

[3] Department of Biological Sciences, University of Delaware, Newark, DE, 19716, USA

* Corresponding Author (Yan Jin), Phone: 302-831-6962, Fax: 302-831-0605, E-mail: yjin@udel.edu

Abstract

A review of current literature shows that considerable uncertainty exists concerning the role of air-water interface (AWI) in colloid transport in unsaturated porous media. This study aimed to elucidate colloid retention at AWI in a model dynamic system at the pore scale. Colloid behavior in a two-phase flow in microfluidic channels was visualized with a confocal microscope. In addition to experiments, numerical simulations of the channel flow field were performed. We found that dispersed colloids did not attach to AWI under the investigated conditions while colloids previously attached to the channel walls could be retained at AWI with capillary forces during AWI passage and be further transported with the AWI. Air front (receding AWI) was more efficient than water front (advancing AWI) in colloid mobilization. The study provides convincing experimental evidence on the mechanisms by which colloid attachment to AWI occurs and clarifies the role that AWI plays in colloid remobilization and transport in unsaturated porous media. In addition, the study clarifies the mechanism of colloid transport to contact line region where colloids can be retained.

1. Introduction

Colloid transport in soil porous media has been drawing considerable scientific attention due to potentially enhanced transport of contaminants associated with mobile colloids [*McCarthy and Zachara*, 1989; *Saiers and Ryan*, 2006; *Sen and Khilar*, 2006]. The interest in colloid transport is additionally intensified by the importance of understanding and predicting microorganism and nanoparticle transport in natural porous media [*Jin and Flury*, 2002; *Ginn et al*., 2002; *Lecoanet et al*., 2004; *Wiesner et al*., 2006]. Unsaturated porous media are more complex systems compared to saturated porous media due to complications arising from the presence of air phase and additional colloid retention regions: air-water interface (AWI) and contact line (where air, water, and solid meet). The presence of AWI may increase or decrease colloid transport substantially, e.g., by serving as a colloid carrier [e.g., *Goldenberg et al*., 1989; *Wan et al*., 1994] or by being a dynamic physical barrier [*Auset et al*., 2005]. While some researchers have shown that dispersed colloids deposit on the contact line during AWI movement [e.g., *Crist et al*., 2005; *Lazouskaya and Jin*, 2008], moving air-water interfaces have been additionally emphasized to play a role in mobilizing *in situ* colloids or colloids previously deposited in porous media [*Saiers et al*., 2003]. Therefore, occurrence of multiple processes associated with the presence and movement of AWI requires further evaluation of colloid behavior and its governing mechanisms in that region. Also, it appears that AWI retention and contact line retention are closely related and therefore need to be jointly evaluated.

Colloid interfacial interactions and their role in colloid attachment and retention have been extensively studied under different physicochemical conditions [e.g., *Chen and*

57 *Flury*, 2005; *Kuznar and Elimelech*, 2007; *Lazouskaya and Jin*, 2008]. However, the
58 dynamic nature of the processes in soil porous media implies the presence of moving air-
59 water interfaces and, therefore, necessity of hydrodynamic consideration. It has been
60 recently shown that physicochemical and hydrodynamic processes are essentially coupled
61 in governing colloid behavior in porous media [*Johnson et al*., 2007; *Torkzaban et al*.,
62 2007; *Torkzaban et al*., 2008a], with hydrodynamic effects dominating bulk transport and
63 physicochemical effects controlling the interactions of colloids with the interfaces (e.g.,
64 SWI, AWI, and the contact line). Namely, forces of hydrodynamic and physicochemical
65 origins acting on a colloid can each be important depending on the relative location of the
66 colloid at the pore scale. The flow field and geometry of porous media define colloid
67 trajectory and thus play an important role in immobilization or mobilization of colloids
68 due to hydrodynamic flow pattern [*Torkzaban et al*., 2008b]. In addition to macroscopic
69 flow field (at the pore and sample scales), the effect of hydrodynamics on colloid
70 interactions with AWI at microscopic (colloid) scale has been demonstrated in atomic
71 force microscopy (AFM) studies where a higher short-ranged hydrodynamic repulsive
72 force was measured upon increased approach velocity of a colloid toward AWI
73 [*Nalaskowski et al*., 2002; *Johnson et al*., 2006].

74 Due to the complexity of colloid retention and transport processes and multiple
75 parameters affecting them, a considerable portion of colloid transport research has been
76 conducted employing pore-scale systems allowing direct visualization of colloid behavior
77 [*Ochiai et al*., 2006]. To date, most of the pore-scale and micromodel studies utilized
78 flow systems (i.e., colloid behavior was observed under flow conditions), and the focus
79 has been placed mostly on colloid retention mechanisms [e.g., *Wan and Wilson*, 1994;

Sirivithayapakorn and Keller, 2003b; *Crist et al*., 2004; *Chen and Flury*, 2005; *Crist et al*., 2005; *Zevi et al*., 2005; *Gao et al*., 2006]. Nevertheless, there have been some reports on hydrodynamic behavior of colloids at the pore scale in saturated systems [e.g., *Sirivithayapakon and Keller*, 2003a; *Auset and Keller*, 2004; *Baumann and Werth*, 2004] and, to a lesser extent, on the importance of hydrodynamics in unsaturated systems [*Gao et al*., 2006; *Lazouskaya et al*., 2006; *Lazouskaya and Jin*, 2008]. In pore-scale studies focusing on unsaturated colloid retention and transport, a number of approaches have been used in introducing the air phase: as mobile and trapped air bubbles [*Wan and Wilson*, 1992; *Wan and Wilson*, 1994; *Sirivithayapakorn and Keller*, 2003b; *Chen and Flury*, 2005; *Gao et al*., 2006], by utilizing open systems [*Crist et al*., 2004; *Crist et al*., 2005; *Zevi et al*., 2005; *Lazouskaya et al*., 2006], and by employing two-phase flows [*Wan and Wilson*, 1993; *Lazouskaya and Jin*, 2008; this study]. The different geometry and hydrodynamics of each system are designed to model different AWI configurations in unsaturated systems. For example, open flow systems represent steady-state flow in unsaturated porous media and flow in corners and grooves in soil while two-phase flow systems represent transient regimes in unsaturated soil media such as during drainage and infiltration. Air bubbles are ubiquitously present in the vadose zone as well as in the saturated zone below water table (*Wan and Wilson*, 1993).

Evaluation of a dynamic air-water interface is closely related to the problem of moving contact line, which has been broadly discussed in the literature [e.g., *Pomeau*, 2002; *Shikhmurzaev*, 2006; *Fuentes and Cerro*, 2007]. Despite extensive research, a complete theoretical description of microscopic contact line behavior is still in progress. Nevertheless, broad industrial applications (e.g., coating and microgravity applications)

have resulted in numerous theoretical and experimental studies of hydrodynamics in the contact line region, e.g., experiments with two-phase flows in circular tubes [*Hoffman*, 1975; *Dussan*, 1977; *Mumley et al*., 1986a; *Mumley et al*., 1986b; *Ichikawa et al*., 1994]. Other related studies, which investigated the motion of bubbles and droplets in square and rectangular channels, have also been reported [e.g., *Kolb and Cerro*, 1993; *Kinoshita et al*., 2007]. *Karnis and Mason* [1967] investigated the movement of large particles (with radii from 35 to 650 μm) near AWI in circular tubes and reported accumulation of particles behind AWI, which was attributed to hydrodynamic interactions as physicochemical forces are unimportant for this range of particle sizes. However, to the best of our knowledge, the specific behavior of colloid-size particles (< 10 μm) in such systems has not been systematically studied.

Interactions of *in situ* or attached colloids with moving AWI and consequent mobilization have been of considerable interest in colloid transport literature (e.g., *El-Farhan et al*., 2000; *Saiers et al*., 2003; *Zhuang et al*., 2007; *Shang et al*., 2008; *Sharma et al*., 2008a; *Sharma et al*., 2008b). Several field and laboratory column studies reported that colloid mobilization occurs both during drainage and infiltration events and depends on irrigation pattern, i.e., increases with flow rate and multiple passages of AWI (*El-Farhan et al*., 2000; *Zhuang et al*., 2007; *Shang et al*., 2008). Extensive research has been conducted to investigate colloid removal with AWI from substrates and from the surfaces in parallel-plate chamber [*Leenaars and O'Brien*, 1989; *Noordmans et al*., 1997; *Gómez Suárez et al*., 1999a; *Gómez Suárez et al*., 1999b; *Gómez-Suárez et al*., 2001a; *Gómez-Suárez et al*., 2001b; *Sharma et al*., 2008b] providing valuable information on parameters

that define colloid mobilization with AWI; however, direct colloid-scale observation of this process has not been reported.

In this study, we used a microfluidic channel with an angular (trapezoidal) cross section to represent a soil capillary [*Lazouskaya and Jin*, 2008]. A moving AWI was created as the phase boundary of the two-phase flow in the channel and visualized with a confocal microscope. With this system, we aimed to obtain information on colloid behavior in the vicinity of AWI and in the contact line region under dynamic conditions. Both advancing and receding cases were considered, and the major emphasis was on evaluating the hydrodynamic condition in the interfacial regions and its role in colloid retention at AWI or remobilization by AWI. In addition, by direct observation of colloid behavior, information on occurrence and interplay of several concurrent mechanisms involving both dispersed and attached colloids was obtained. The experimental observations were considered and explained through analysis of the forces acting on colloids in each case.

2. Materials and Methods

Colloids utilized in this study were yellow-green fluorescent carboxylate-modified polystyrene microspheres with an average diameter of 500 nm and particle density of 1.055 g/cm^3 (F8813, Molecular Probes, Eugene, OR). All colloid suspensions were prepared by dispersing the microspheres in de-ionized (DI) water to final concentrations of 2 ppm and 4 ppm, or 2.9×10^7 and 5.8×10^7 particles/ml, respectively. Colloid zeta-potential in DI water was measured as -65.6 ± 2.3 mV using Zetasizer Nano ZS (Malvern Instruments, Westborough, MA). The Hückel's approximation in the determination of

148 zeta-potential was assumed, which is more applicable for the case of thick electric double
149 layer of colloids in DI water [*Ross and Morrison*, 1988]. Carboxylate-modified colloids
150 can be characterized as hydrophilic, i.e., with contact angle < 30° [*Petkov and Denkov*,
151 2002]. The experimental conditions (i.e., colloid concentration as well as colloid and
152 solution chemistry) were chosen to minimize colloid-colloid and colloid-wall attractive
153 interactions, which would allow reusing the microfluidic channels. In this study, the
154 hydrophilic carboxylate-modified colloids dispersed in DI water were employed thus
155 presenting the case of minimized hydrophobic attraction and maximized electrostatic
156 repulsion. The size of colloids was chosen sufficiently small so that it could be assumed
157 that gravity effect is insignificant and that the flow field is not affected by the presence of
158 the particles.
159 Microfluidic channels (Microfluidic ChipShop, Jena, Germany) are made of
160 poly(methyl methacrylate) (PMMA) and have a trapezoidal cross section with base
161 widths of 42 and 70 μm and height (depth) of 20 μm. The length of the microfluidic
162 channels is 85 mm. The acute angle of the trapezoidal cross section is 54.7° as shown in
163 Fig. 1A (right). For each experiment with confocal microscope, the channel was
164 positioned in a way that the microscopic observations occurred through the wider base
165 (70 μm). Experimental procedure included pumping of dilute (2 or 4 ppm) colloid
166 suspension through a microfluidic channel with a syringe pump and concurrent
167 observation of colloid behavior at the point of interest with a confocal microscope (Carl
168 Zeiss Axiovert 200M equipped with LSM 510, Oberkochen, Germany) employing a 10×
169 magnification lens.

To observe the behavior of colloids in the interfacial regions, the air-water interface was created by pumping colloid suspension into an empty (dry) channel and establishing the liquid front in the observed area of the channel. The employed syringe pump (PHD 22/2000, Harvard Apparatus, Holliston, MA) has the ability to work in both infusing and withdrawing modes thus allowing movement of the observed front in both directions, creating two regimes of the moving air-water interface: liquid phase displacing air phase (water front) and air phase displacing the liquid phase (air front). The range of flow rates employed at different stages of an experiment was from 0 ml/h (with the pump stopped) to 0.05 ml/hr; most of the confocal images were recorded between 0 and 0.002 ml/h. Examples of confocal images of water and air fronts in the channel are shown in Fig. 1 (A and B). The notable difference between the two regimes is the presence of residual saturation following the movement of the air front, which is shown schematically in cross section in Fig. 1B.

The images were recorded at the speed of 2 frames/s with a resolution of 1024×130 pixels and were followed with image processing using confocal integrated software (Zeiss LSM) and advanced imaging software Volocity 3.0.1 (Improvision, Inc.). Image processing was employed to acquire quantitative information on the front and colloid velocities and qualitative information on colloid behavior and retention as well as to perform particle tracking. Colloid locations in *z*-direction, which is perpendicular to the observation, could not be precisely resolved because of the relatively thick imaging optical section (6–7 μm). Additional information on optical characteristics of the system as well as image acquisition and processing can be found in our previous work [*Lazouskaya et al*., 2006; *Lazouskaya and Jin*, 2008].

Front (AWI) velocities were obtained from the recorded images and varied from 0.2 to 50 μm/s. However, the majority of the recorded images had front velocities in the range from 5 to 13 μm/s. These front velocities correspond to the transitional flow rate between 0.002 ml/h (the lowest pump setting with the current setup) and 0 ml/h and have been recorded after the pump was stopped. Due to the slow response of the front velocity to the changes in a pumping flow rate, the front velocities were nearly constant during the observation time.

All experimental observations were divided into three groups and considered separately in subsequent discussions: observations of the flow field, interactions of dispersed colloids with dynamic AWI (moving front), and interactions of attached colloids with dynamic AWI.

3. Results and Discussion

3.1. Flow Field in the Microfluidic Channel

3.1.1. Experimental Observation of Flow Field near the AWI

The bulk aqueous flow in the trapezoidal channel observed at some distance from AWI (e.g., ~ 400 μm, or ~ 10*a*, at the front velocity of 12 μm/s where *a* is the channel characteristic width) can be characterized visually as a laminar flow with a quasi-parabolic velocity profile. However, we observed that the flow field had a complex pattern in the vicinity of AWI where colloids followed the flow streamlines and exhibited circular motion with respect to AWI. Similar flow patterns have been earlier reported for two-phase flows in circular capillaries [e.g., *Karnis and Mason*, 1967; *Dussan*, 1977; *Ichikawa et al*., 1994]. The observed flow field relative to AWI for both water and air

fronts is shown schematically in Fig. 2. Additional information on flow patterns for water and air fronts can be found in supplementary material (Movie 1.avi and Movie 2.avi) where colloid tracking was implemented with Volocity 3.0.1 to visually emphasize the complexity of flow in the vicinity of AWI.

Because AWI was moving, the absolute colloid velocities could be viewed as a superposition of colloid velocities relative to AWI and the constant advancement velocity of the AWI. Namely, colloid velocity relative to AWI is determined as the difference between the absolute colloid velocity (velocity relative to channel wall) and the front (AWI) velocity. The schematic flow pattern shown in Fig. 2 was constructed using these relative colloid velocities.

Fig. 2 shows that colloid movement relative to AWI changes its direction when a colloid approaches the AWI, due to transition from a quasi-parabolic axial (y-component) flow velocity profile to a nearly uniform axial velocity profile at AWI. This necessarily leads to transverse motion of colloids. Fig. 2 is schematic and the size of arrows shown does not reflect the magnitudes of colloid velocities. Also not shown in Fig. 2 are some experimentally observed random movement of colloids and variations in their paths relative to AWI, likely due to Brownian motion, which is notable for the relatively small (500-nm) colloids used in this study, especially at lower front velocities. Some colloids made apparent transfers between streamlines, which resulted in visual re-circulation of those colloids in regions close to AWI.

In the central region of the channel, colloids moved predominantly in the same direction as the AWI. This implies that colloid velocities relative to AWI are smaller compared to their absolute velocities. The relationship between the water front velocity

and absolute colloid velocities measured based on the recorded images is illustrated in Fig. 3 where velocities of colloids approaching the water front are plotted against the front velocity. Fig. 3 demonstrates that, at a given front velocity, the absolute velocities of approaching colloids exhibit a distribution of values, which depend on the position of the colloids in respect to the front and to the walls (or channel center). These values are greater than the water front velocity (the straight line in Fig. 3), which illustrates that most of the colloids approached AWI at velocities exceeding the water front velocity. The slower colloid velocities correspond to colloids positioned closer to the channel wall and possibly changing their direction relative to AWI. In general, colloids had higher velocities in the center of the channel and slower velocities close to the channel walls.

For the air front case, central colloids experience apparent retardation as the distance between colloids and AWI decreases. The absolute trajectories of colloids are shown in Fig. 4 where colloid trajectories are imposed on the channel image; colloids are located at different initial distances from air front, and the moving air front is not shown. Fig. 4 shows that colloids sufficiently far from the front ($> \sim 400$ μm) were not affected by it and were considered to be in bulk flow while colloids closer to AWI demonstrated more complex behavior when approaching AWI. In addition, Fig. 4 demonstrates that both magnitude and direction of colloid velocities were affected by their interactions with the front. Colloids slowed down as they approached AWI and then accelerated after interaction with AWI until reaching the steady-state velocity of the bulk flow. The interactions of colloids and AWI in this case include both hydrodynamic (viscous) and colloid interactions, which are considered in more detail in Section 3.2.

3.1.2. Theoretical Treatment of Single-Phase Flow Velocity Distribution in the Trapezoidal Channel

To understand the velocity distribution in the trapezoidal channel far away from the AWI, we solved (single-phase) viscous flow in the channel using both an analytical method and a numerical (lattice-Boltzmann, or LBM) approach. Detailed description of the two modeling approaches and comparison of their simulation results are given in Appendix A. Fig. 5 shows model-simulated contour of the axial, or *y*-component, velocity normalized by its maximum in the cross section of the channel. It is clearly observed that the effect of no-slip wall boundary condition is accurately represented. As shown in the simulated flow distribution, the axial velocity reaches its maximum value near the center of the channel cross section and decreases gradually toward the channel walls. Furthermore, at the two sharp corners (with acute interior angle) along the bottom wall, velocities are very low due to the combination of strong viscous effect and no-slip walls. The obtained theoretical solution is in qualitative agreement with experimental observations.

The simulated results of single-phase flow field in the channel provide better understanding of two-phase flow behavior such as the presence of the residual liquid trapped in these two corners for the air front case (Fig. 1B). This can be qualitatively explained as the strong surface tension effect acting on the meniscus-trapped fluid, relative to the viscous force due to the walls. The trapping is unavoidable in these corners since the surface tension effect increases with decreasing size of the meniscus trapped fluid and, at the same time, the bulk flow velocity in the corners is very small as shown by the single-phase model result.

3.1.3. Theoretical Flow Streamlines near a Moving AWI in a Two-Dimensional (2D) Channel

To gain a better understanding of the observed colloidal movement near AWI, preliminary simulation of the flow field near a moving AWI and contact line in a two-dimensional (2D) channel was performed using the multiphase LBM method of *Kang et al*. [2004]. The simulation domain contains a long channel where the interface is initially placed at a quarter of the channel length. Similar to the study of *Kang et al*. [2004], the flow is driven by a prescribed parabolic inlet and outlet velocity profile (see Appendix B, Fig. B1 for more details). The fluid viscosity and surface tension were set to yield a capillary number of Ca = 0.021 and a Reynolds number of Re = 10.67. Capillary number is the ratio of viscous and surface tension forces, and Reynolds number characterizes the ratio of inertial and viscous forces [*Atencia and Beebe*, 2005]. The densities and viscosities of the two fluids were assumed to be the same in these preliminary simulations, due to a numerical stability issue for high density ratio [*Kang et al*., 2004; *Yuan and Schaefer*, 2006]. Assuming a characteristic channel width of a = 40 μm, the capillary number is $Ca = 1.24 \times 10^{-7}$, the Reynolds number is $Re_w = 4.47 \times 10^{-4}$ on the water side and $Re_a = 2.58 \times 10^{-5}$ on the air side, the kinematic viscosity ratio is $\nu_w / \nu_a = 0.058$, and the density ratio is $\rho_w / \rho_a = 846.6$. Although the parameters used in modeling do not match the parameters in the experiments, we note that the simulated flow is mostly governed by surface tension with $Ca << 1$, which is qualitatively similar to the experiment. For a straight channel considered in the simulation, the flow Reynolds number is not expected to have any significant effect. Therefore, the simulated results are of qualitative value in interpreting the experimental observations.

We performed flow simulations for two scenarios: a water front where flow is directed from right to left, corresponding to the scenario shown in Fig. 2A, and an air front where flow is directed from left to right, similar to Fig. 2B. The simulation details are provided in Appendix B. We now examine the flow field relative to the moving contact line, that is, the resulting flow field after the mean flow speed is subtracted, and Fig. 6 shows this relative flow on the water side for both the air front and the water front cases. Due to the symmetry of simulated flow, only half of the channel near the interface is shown. For the air front case, the relative flow on the water side (right to the interface) points into the interface near the center of the channel, but points away from the interface near the wall. The opposite is shown for the air front case, where the flow near the center moves away from the interface and it moves into the interface near the wall. These different relative flow patterns are consistent with the colloid trajectories relative to the interface observed in the experiments (Fig. 2). The simulations provide additional detail of the flow near the AWI: a stronger transverse flow is seen for the air front case than the water front case, due to a higher front inclination for the former case. This transverse flow could generate viscous drag normal to the channel wall and help mobilize previously attached colloids when the AWI in the air front case is passing through.

3.2. Interactions of Dispersed Colloids with Moving AWI

3.2.1. Experimental Observation of Colloid Movement and Retention

Colloids were observed to closely approach both air and water fronts at different front (AWI) velocities thus creating conditions for colloid interactions with AWI. At low front velocities, convection of colloids toward AWI was reduced, and the approach

occurred mainly due to Brownian motion. At faster front velocities, colloids approached AWI following streamlines, shown schematically in Fig. 2, and slid along AWI before they returned to the bulk solution. Also, colloids were observed to approach AWI and return back to the bulk solution without noticeable movement along or interaction with the AWI. This is likely due to the possible movement of colloids in *z*-direction (perpendicular to the image), which could not be sufficiently resolved with the current experimental system.

The duration of colloid sliding along or residing close to a water front varied from 0.5 to 12 s, which could be attributed to the different hydrodynamic paths the colloids followed or to possible temporary association with AWI. The temporary association of colloids with AWI can generally stem from colloid-AWI interactions [*Lazouskaya and Jin*, 2008] as well as from diminished relative velocity between colloids and the AWI. In case of an air front, colloid sliding times could not be precisely determined due to the frequent involvement of the sliding colloids into the corner regions (Fig. 2B). The permanent or long-term (longer than observation time) retention of dispersed colloids at AWI was not observed for either air or water front. This is consistent with the net repulsive interactions between colloids and AWI under the employed experimental surface and solution chemistry conditions [*Lazouskaya and Jin*, 2008].

Presence of residual saturation in the corner region upon an air front passage allows flow and consequently colloid movement into the region. The movement of colloids occurs in the direction opposite to the air front movement, and colloids attain high velocities in that region (Fig. 2B). A closer view of the corner region is provided in Fig. 7 where both an image of air front and a schematic cross section of the corner with possible

353 colloid locations are shown. Colloid movement in the corners likely occurred in the bulk
354 (Fig. 7, position 3). Some colloids were also observed to transport in the corner in the
355 direction of air front movement, which can be viewed in supplementary material (Movie
356 3.avi). In this case, colloids were probably transported either at AWI of the corner region
357 (Fig. 7, position 2) or on the contact line along the smooth surface (Fig. 7, position 1).
358 This may also be related to the previous observations of reverse flow at AWI in an open
359 capillary channel [*Lazouskaya et al*., 2006]. Direct retention of dispersed colloids in the
360 very corners of the channel was also observed (Fig. 7, position 4). However, this was not
361 a common observation and mostly occurred at low flow velocities. Such retention could
362 be attributed to random retention by wedging or straining [*Bradford et al*., 2006; *Johnson*
363 *et al*., 2007; *Bradford and Torkzaban*, 2008]. Some colloids retained in the very corners
364 were previously retained on the channel wall and pushed to the corner location with the
365 air front at higher flow rate, which demonstrates another mechanism of enhanced
366 straining in unsaturated porous media in addition to previously acknowledged
367 hydrodynamically favorable conditions such as zero velocity on the solid and flow
368 pattern in straining locations [*Bradford and Torkzaban*, 2008; *Torkzaban et al*., 2008b].
369 Behavior and location of the retained colloids shown in Fig. 7 are additionally discussed
370 in Section 3.3.1.

371 In addition to AWI, contact line (located where AWI contacts channel wall) is
372 another site for potential colloid retention. In the case of an air front, the corners of
373 residual saturation provide additional regions where colloids could be involved with the
374 flow. In the absence of residual saturation (e.g., a water front), the contact line in the very
375 corner was a preferred location of retention due to low flow velocities in that region;

however, at higher velocities many colloids were diverted from such retention (Fig. 2). In general, contact line serves as a more favorable retention site compared to AWI for dispersed colloids because colloids can slide along AWI to the contact line and be retained.

Although experimental observations suggest that hydrodynamic flow pattern plays an important role in colloid behavior, colloidal forces cannot be ignored and are discussed in Section 3.2.2, which provides more quantitative consideration of colloid interactions with AWI.

3.2.2. Equation of Colloid Motion

The typical values of parameters, determined from the experiments or obtained from the literature, that were used in the calculations of this and subsequent sections are provided in Table 1. In addition to Reynolds (Re) and capillary (Ca) numbers introduced in Section 3.1.3, Peclet (Pe) number provides information on the relative importance of convection and diffusion [*Franzini and Finnemore*, 1997; *Atencia and Beebe*, 2005]. More detailed description of Reynolds, Peclet, and capillary numbers can be found elsewhere [*Atencia and Beebe*, 2005]. Under the experimental conditions of this study, the Peclet number was determined as Pe = 2.5. The small Peclet number points at the importance of diffusion; therefore, Brownian motion has to be taken into account while considering colloid motion.

There are a number of forces (including colloid and hydrodynamic) acting on a dispersed colloid as it approaches AWI. The problem of particle capture on spherical or cylindrical collectors has been extensively discussed in the literature [e.g., *Spielman and Goren*, 1970; *Yao et al*., 1971; *Spielman*, 1977]. These results obtained for solid

collectors can be applied to colloid interactions with AWI. For example, the treatment of solid collectors has been previously applied to interactions of particles and air bubbles in flotation [*Schulze*., 1984]. In the case of surfactant-free (mobile) bubbles, the required driving force for a particle to approach the bubble is four times smaller than in the case of rigid (surfactant-modified) bubbles [*Schulze*, 1984]. Theoretical studies have shown that hydrodynamic resistance of a free interface (e.g., AWI) at a very close approach as compared to solid surfaces can be up to 10 times smaller [*Happel and Brenner*, 1973; *Warszynski*, 2000]. In our case, the air or water front (AWI) played a role of a collector; similarly to the approximation used by *Nalaskowski et al*. [2002], AWI was treated as a solid surface in this study.

The problem is additionally complicated with the fact that AWI is moving. The colloids located close to the channel center moved mostly in the same direction with the front, which implies that the velocity of colloids relative to the front could be substantially reduced as discussed in Sections 3.1.1 and 3.2.1. Therefore, the relative motion of colloids in respect to AWI has to be considered.

Equation of motion of a colloid approaching AWI includes net gravity force, Brownian force, colloid forces between a colloidal particle and AWI, and hydrodynamic forces and can be written as [*Nguyen and Schulze*, 2004; *Johnson et al*., 2007]:

$$m\frac{d\vec{v}}{dt} = -\frac{1}{2}m_f\frac{d\vec{v}}{dt} + \vec{F}_D + \vec{F}_{col} + \vec{F}_{Br} + \vec{F}_G \qquad (1)$$

where the first term on right hand side is the added-mass term, $\vec{F}_D$ is the drag force, $\vec{F}_{col}$ represents colloid forces including electrostatic, van der Waals, and hydrophobic forces,

$\vec{F}_{Br}$ is the force due to Brownian motion, and $\vec{F}_G$ is the net gravity force. The symbol m denotes the mass of the particle, and m_f denotes the mass of the fluid, which volume equals to the volume of the particle; $\vec{v}$ is particle velocity. The Basset force was not considered in the equation because it does not make a substantial contribution in case of small particles [*Nguyen and Schulze*, 2004]. Similar to *Johnson et al*. [2007], any possible inertial effects of colloid motion have been accounted for in the acceleration term, and the errors associated with the use of hydrodynamic corrections derived for inertia-free systems are considered small. Similar to the convention used in energy calculations, the positive and negative signs of the force indicate repulsion and attraction, respectively. More detailed consideration of forces in Eq. (1), employed expressions, and colloid-AWI geometry is provided in Appendix C.

The calculated drag force, colloid forces, force due to Brownian motion, and gravity force (for reference) at colloid approach velocity of 10 μm/s are plotted in Fig. 8. Fig. 8 illustrates the relative magnitudes of the forces as a function of dimensionless separation distance $H = h/r$ between colloids and AWI where h is separation distance and r is colloid radius. As it can be inferred from the graph, most of the forces (with the exception of randomly directed force of Brownian motion) acting between colloids and AWI are repulsive.

It should be noted that the drag force appears to be long-ranged in the graph although it is expected to be insignificant (e.g., compared to Brownian force) at the distance of 2-3 particle radii, or 2-3 H [*Goren and O'Neill*, 1971]. Due to the small density contrast between colloids and the water solution and the small size of colloids, the effective inertial response time of a colloid is very small. As a result, a colloid located

445 away from a surface or AWI tends to closely follow the fluid streamlines if the Brownian
446 motion is not considered. In this sense, a colloid can be viewed as a tracer particle for the
447 bulk flow. The small colloid size, however, implies that the Brownian motion is effective
448 in dispersing colloids in the bulk flow. Consequently, a finite drag force is always present
449 in response to the Brownian motion. In addition, the drag force acting on a colloid close
450 to AWI can be attractive when the colloid is moving away from AWI, but this scenario
451 was not considered in Fig. 8.

452 The calculated Peclet number (Pe = 2.5) points at the importance of Brownian
453 motion. At sufficiently low colloid velocity or taking into account the reduced
454 hydrodynamic resistance of AWI compared to solid surfaces, Brownian motion can be
455 effective in driving a colloid toward AWI, and the possibility of colloid attachment to
456 AWI would be solely determined by the action of colloid forces. The resulting colloid
457 force for the hydrophilic, carboxylate-modified, colloids is repulsive since the
458 hydrophobic force does not make a considerable contribution [*Lazouskaya and Jin*,
459 2008]. For the carboxylate-modified colloids with diameter of 500 nm dispersed in DI
460 water and interacting with AWI, repulsive electrostatic force is in the order of 10^{-11} N and
461 is dominant at the separation distances over 1 nm. At closer distances, calculated van der
462 Waals force and hydrophobic force are stronger in magnitude than electrostatic force;
463 however, van der Waals repulsion dominates the hydrophobic attraction at all distances.
464 For more hydrophobic colloids, some attractive association of colloids with AWI due to
465 hydrophobic force would be more probable (e.g., via secondary minimum), but this
466 possibility is strongly influenced by solution chemistry and is more likely at higher
467 solution ionic strength [*Lazouskaya and Jin*, 2008]. While the attachment of colloids

under the experimental conditions is unlikely, the temporary association of colloids with AWI mentioned in Section 3.2.1 could be due to the action of Brownian motion, flow streamlines in the tangential direction (with less hydrodynamic resistance as indicated in Appendix C), or possible existence of flow stagnation regions. Therefore, the knowledge of flow field in the interfacial region together with the analysis of physicochemical interactions is essential for providing better understanding of the mechanisms governing colloid behavior close to AWI.

3.3. Interactions of Attached Colloids with Moving AWI

Apart from dispersed colloids, colloids deposited on the walls of the channel as well as attached at AWI and contact line were present. The colloids that deposited on the wall came mostly from the bulk solution, but some also originated from the retained colloids on the contact line. As described in the previous section, stable retention of dispersed colloids at AWI is unlikely. Nevertheless, colloids attached at AWI permanently have been clearly observed in the experiments. Therefore, it suggests that colloids attach to AWI not as dispersed colloids, but as a result of involvement of previously deposited colloids with the front (AWI). This may be attributed to secondary-minimum retention of colloids on the wall where the associated adhesive force is weaker than the force exerted by approaching AWI. As illustrated in Fig. 7, the observed locations of colloid attachment in the channel are on the wall, at AWI, and on the contact line. This is generally true for both air and water fronts.

There are a number of ways the previously-deposited colloids can be affected by the passage of a moving front (AWI). The deposited colloids can: (1) be involved and

transported with the front (AWI) as illustrated with the supplementary material (Movie 4.avi); (2) be shifted with the front toward the corner region (e.g., the colloid follows the front along the surface in the direction indicated with the white arrow in Fig. 7 until reaches the corner region where upon the front passage it is held in position 1, Fig. 7), which is more characteristic to air front than water front due to the difference between the advancing and receding contact angles and the associated contact line curvature; (3) be remobilized back into the bulk solution upon interaction with the front; and (4) remain unaffected on the wall. The behavior of attached colloids upon passage of a moving AWI is determined by the fine force balance between colloid, channel wall, and AWI interactions. Depending on the conditions and parameters under consideration, which often exhibit a broad distribution at the colloid scale, a number of different mechanisms (e.g., the outlined above cases 1-4) have been shown to occur.

3.3.1. Efficiency of Colloid Detachment by the Moving AWI

To explain the observations and the differences between the cases of attached colloid involvement with AWI and shifting with the air front (cases 1 and 2 listed above), the forces acting on a colloid are considered.

Colloid positioning relative to an air front and major forces acting on a colloid are schematically shown in Fig. 9, in which the interaction geometry for a colloid deposited on the channel wall and for the air front is shown. In Fig. 9A, the angles φ and θ denote the receding contact angle on the wall (PMMA) and colloid contact angle, respectively. The values of the angles φ and θ are provided in Table 1. Fig. 9B proposes a mechanism illustrating case (1), i.e., detachment of a deposited colloid by AWI.

513 The major forces acting on the colloid in this case are colloid forces between the
514 colloid and channel wall (PMMA) F_{col}, drag force F_D, and surface tension (capillary)
515 force F_σ. A transverse component of the drag force due to the flow field close to AWI
516 (Figs. 2 and 6) could also act on the colloid and contribute to colloid detachment in air
517 front case, but is not considered in Fig. 9. Colloid forces between colloids and PMMA
518 were estimated using the same treatment utilized for colloid-AWI interactions. While the
519 exact value of PMMA surface potential is not known, it was assumed as -25 mV [*Lubeck*
520 *et al*., 2003] and the order of the total colloid interaction force was determined as 10^{-10} N
521 or smaller. Experimental observations (cases 2 and 3, in particular) suggest that
522 secondary-minimum retention is the likely mechanism of colloid retention on the wall
523 although this cannot be proved by DLVO calculations, which could be due to uncertainty
524 associated with the PMMA surface potential value used. The estimate for the drag force
525 in *y*-direction was performed using the expression $F_D = 6\pi\mu r v_{front}$ and was determined in
526 the order of 10^{-14} N. The viscous (drag) force, which appears upon colloid removal from
527 the surface in *z*-direction, was not considered [*Leenaars and O'Brien*, 1989]. Earlier, a
528 trivial effect of viscous drag force on colloid detachment compared to surface tension
529 force has been reported [*Gómez Suárez et al*., 1999a].
530 The maximum surface tension force in *z*- and *y*-directions illustrated in Fig. 9A (air
531 front) can be determined as [*Leenaars*, 1988; *Noordmans et al*., 1997]:
532

533 $$F_\sigma^z = -2\pi r\sigma \sin^2\left(\frac{\pi+\theta}{2}\right)\cos\varphi \qquad (2)$$

534 $$F_\sigma^y = -2\pi r\sigma \sin^2\left(\frac{\pi+\theta}{2}\right)\sin\varphi \qquad (3)$$

where σ is the fluid (water) surface tension, θ is colloid contact angle, and φ is PMMA receding contact angle (for air front). Using the values in Table 1, surface tension force components F_σ^z and F_σ^y were determined as -6.6 × 10^{-8} N and -8.6 × 10^{-8} N, respectively. Therefore, surface tension force is the dominant force acting on the particle. In particular, the *y*-component of the surface tension force dominates all other forces in (negative) *y*-direction; this explains the observed shifting of the particle along the smooth channel surface (case 2).

Colloid transfer from the contact line to AWI (case 1 or Fig. 9B) cannot be predicted from the analysis above and Fig. 9A due to the absence of a governing repulsive force in *z*-direction, but may occur when colloid forces are too weak to maintain the colloid attached to the solid, e.g., due to surface charge heterogeneity, mechanical irregularities, or possible hydrodynamic disturbances. Surface irregularities may result in regions of higher and lower repulsion [*Bowen and Doneva*, 2002]. *Butt et al*. [2005] reported lower colloid-surface adhesion measured with AFM than predicted theoretically, which was attributed to surface roughness. Some researchers have reported increased deposition of colloids compared to theoretical prediction due to surface charge heterogeneity [*Sjollema and Busscher*, 1989; *Suresh and Walz*, 1996; *Hoek et al*., 2003]. Although hydrodynamic patterns in the contact line region have been broadly investigated, accurate description of hydrodynamics in that region has not been developed. There have been reports of a rolling motion in close proximity of an advancing interface [e.g., *Dussan*, 1979; *de Gennes*, 1985; *Pismen*, 2002]. The mobile AWI in our case would make the AWI and colloids at AWI very susceptible to any

hydrodynamic disturbance [*Roizard et al*., 1999]. The complex flow field close to the contact line (Fig. 2) coupled with weak adhesion to channel wall are likely causes of the observed colloid detachment and its subsequent movement with AWI (Fig. 9B). The illustration of this process can be viewed in supplementary material (Movie 4.avi).

The prerequisite for occurrence of scenarios (1) and (2) is the strong attachment of the colloid to the channel wall to allow formation of a three-phase contact upon front passage. When colloid-PMMA interactions are not sufficiently strong, the repulsive forces between colloids and AWI will cause remobilization of colloids from the wall back into solution, which has been experimentally observed (case 3). Regarding case (4), the stable colloid attachment on the wall possibly occurred in the primary minimum.

For water front (Fig. 9C), while colloid forces and drag force in *y*-direction are the same as for air front (Fig. 9A), the surface tension force is different. The maximum surface tension force (in *z*- and *y*-directions) exerted on a colloid in Fig. 9C can be determined as [*Leenaars*, 1988; *Noordmans et al*., 1997]:

$$F_{\sigma}^{z} = 2\pi r\sigma \sin^{2}(\frac{\theta}{2})\cos\varphi \qquad (4)$$

$$F_{\sigma}^{y} = 2\pi r\sigma \sin^{2}(\frac{\theta}{2})\sin\varphi \qquad (5)$$

where φ is PMMA advancing contact angle (for water front). The calculated surface tension forces for water front are 6.5×10^{-10} N and 3.3×10^{-9} N in *z*- and *y*-directions, respectively. Comparison with the surface tension force values for air front (-6.6×10^{-8} N and -8.6×10^{-8} N in *z*- and *y*-directions) shows that the surface tension forces for water

front are much weaker in both in *z*- and *y*-directions. For water front, the surface tension force in *z*-direction is of the same order of magnitude as colloid forces, thus water front is less effective in mobilizing deposited colloids than air front, which was also observed experimentally and will be discussed further in the following section.

3.3.2. Efficiency of Colloid Transport with the Moving AWI

Colloids permanently attached to AWI can be transported along the channel for sufficiently long times (at least 45 min as experimentally observed) both with air and water fronts. However, this form of transport is quite limited for a number of reasons including the limited area of AWI available for carrying colloids and possible detachment of colloids from AWI along the front passage.

For an air front, no detachment of colloids from AWI was observed. However, due to the presence of residual saturation in corner regions, colloid at AWI could be involved with the flow in those regions and be transported in the corners (Fig. 7, position 2) while attached to AWI. As shown with the air front streamlines in Fig. 2B, flow in the corners occurs in the direction opposite to the front movement. Colloids in the corners (still attached to AWI) move until the flow in that area ceases. Therefore, possible further colloid behaviors include retention on the contact line (e.g., Fig. 7, position 1), retention on the channel wall or in the corner (Fig. 7, position 4) if the liquid phase declines, e.g., as a result of drainage or evaporation, or return back into the solution upon an infiltration event. These possibilities depend on the particular scenarios and affect the total colloid transport with an air front, generally decreasing its effectiveness. Therefore, although a possible transport mechanism, transport with air front was found to account for only a small fraction of colloids under the conditions employed in this study. Nevertheless,

603 direct observation of colloid mobilization and transport with AWI can be viewed in
604 supplementary material (Movie 5.avi and Movie 6.avi) showing colloids at moving AWI
605 at early and later times. Mobilization by downward (air) front has been measured by
606 *Saiers et al*. [2003] in drainage experiments with sand-packed laboratory columns, which
607 was attributed to the action of surface tension forces.

608 Although no residual saturation is present in the case of a water front, colloid re-
609 deposition from AWI to the contact line and to the channel wall was a common feature
610 observed for water front but not for an air front. This difference can again be explained
611 by comparing the surface tension forces acting on colloids in both cases (Figs. 9A and
612 9C). As it has been shown earlier, the surface tension forces in both *z*- and *y*-direction for
613 water front are weaker than for air front and are of the same order of magnitude as the
614 colloid force. This explains not only the less efficient colloid mobilization by water front
615 but also the observed colloid deposition from the contact line on the wall. This implies
616 that the efficiency of a water front in transport of colloids is diminished by both the lower
617 surface tension force for colloid involvement and the possibility of losing the particles. It
618 should be noted that a direct comparison of colloid collection between air and water front
619 is not possible due to unequal experimental conditions: air front interacts with a greater
620 number of colloids, which have been likely deposited recently (interaction in liquid
621 phase), while water front interacts with fewer colloids previously retained in the channel
622 (interaction in air phase). Nevertheless, the efficiency of air or water front to collect and
623 transport attached particles can be judged based on experimental observations and
624 theoretical considerations, both indicate that water front is less efficient in involving
625 attached colloids and more likely to release the particles than air front. The observation of

626 the flow field near AWI (Figs. 2 and 6) provides additional support for the higher air
627 front efficiency in colloid collection: the relative flow in the liquid phase in case of an air
628 front is directed from the wall to the center and contributes to colloid detachment while it
629 is opposite for a water front. These results are consistent with recent findings of *Cheng*
630 *and Saiers* [2008] who found more significant soil colloid remobilization during drainage
631 (analogous to the air front scenario) than during infiltration (water front) in column
632 experiments.

633 Another scenario of water front behavior, which was not considered in this study,
634 includes water front movement in a previously wet channel. While surface tension force
635 plays a similar role as in the initially dry channels, mobilization of colloids previously
636 retained in regions of residual saturation and liquid films may be considerable [*Auset et*
637 *al*., 2005; *Shang et al*., 2008] and can occur with water front in this case.

638 **3.3.3. Effect of Velocity on Interactions of Attached Colloids and the**
639 **Moving AWI**

640 Kinetic effects can play an important role in interactions of attached colloids with
641 AWI. *Leenaars* [1988] reported that almost no colloids were removed at front velocities
642 in the order of several cm/s compared to 70-97% removal at a much lower front velocity
643 of 3 μm/s. The front velocities in this study ranged from 0.2 to 50 μm/s, and no
644 qualitative difference between detachment mechanisms and colloid behavior relative to
645 the front was observed. Apart from the small velocity range tested the observed lack of
646 velocity effect could be also due to small investigated representative area. Higher front
647 velocities were not investigated due to limited imaging speed with the current
648 experimental setup.

649 The analysis in Section 3.3.1 shows that the magnitude of the surface tension force
650 acting on a colloid particle is affected by the dynamic contact angle on channel wall.
651 According to existing empirical expressions, the value of dynamic contact angle is related
652 to the front velocity via capillary number [*Hoffman*, 1975; *Tanner*, 1979]; therefore, the
653 effect of front velocity on colloid removal is likely connected to the change in dynamic
654 contact angle value [*Leenaars and O'Brien*, 1989].
655 Determination of dynamic contact angles is a complex theoretical problem [e.g.,
656 *Shikhmurzaev*, 2006]. Complexity arises from the difficulty determining the exact
657 position of contact line due to existence of precursor film originating from interactions
658 between solid and liquid and unconventional hydrodynamics in the contact line region
659 [*de Gennes*, 1985]. Extensive experimental investigation has been performed using
660 advancing interfaces and photographic techniques [e.g., *Hoffman*, 1975; *Dussan*, 1979;
661 *Fermigier and Jenffer*, 1991], and some empirical relationships between advancing
662 contact angle and capillary number have been developed [e.g., *Hoffman*, 1975; *Tanner*,
663 1979; *Fermigiere and Jenffer*, 1991; *van Remoortere and Joos*, 1991; *Kalliadasis and*
664 *Chang*, 1994], which allow estimation of the dynamic advancing contact angle for a
665 moving interface based on its value at zero front velocity and on capillary number. While
666 these models mostly deal with advancing contact lines, receding contact angles are
667 treated by considering air phase as the advancing fluid [*Fermingier and Jenffer*, 1991].
668 The estimates of dynamic contact angle obtained with models of *Fermigiere and*
669 *Jenffer* [1991], *van Remoortere and Joos* [1991], and *Kalliadasis and Chang* [1994] vary
670 within 1° for the range of velocities from 1 to 50 μm/s, which is consistent with our
671 observations. However, this is not sufficient proof of the governing effect of dynamic

672 contact angle. In previous studies that investigated colloid removal with air bubbles at
673 velocities in the range of $2.37 \times 10^{-3} – 15 \times 10^{-3}$ m/s (much higher velocity regime than in
674 present experiments), the observed lower removal at higher velocities was attributed to
675 insufficient induction time needed to form a three-phase contact between colloids and
676 AWI [*Gómez Suárez et al*., 1999b; *Gómez-Suárez et al*., 2001b], but no theoretical
677 confirmation was provided. It has also been suggested that as the thickness of the liquid
678 film increases at elevated velocities the air bubbles become less effective in removing
679 small particles [*Gómez Suárez et al*., 1999a]. This explanation is not consistent with our
680 experimental observations where, at higher velocities (above 30 μm/s), the residual
681 saturation in corners visually decreased suggesting more contact area between the air
682 front and solid surface. *Sharma et al*. [2008b] conducted experiments on colloid removal
683 with AWI from glass substrates at the velocities in the range of 0.4 – 400 cm/h (or, ~ 10^{-6}
684 – 10^{-3} m/s) and reported a general decrease of colloid removal with velocity; however,
685 the relationship between colloid removal and AWI velocity was also non-linear. Based on
686 their column experiments, *Saiers et al*. [2003] suggested the opposite trend, i.e., increased
687 colloid removal at higher velocities. Such inconsistent reports found in current literature
688 suggest the need of more systematic investigation on the effects of velocity on
689 interactions between attached colloids and AWI, in particular, with velocity regimes
690 characteristic to natural porous media (~ 10^{-5}–10^{-4} m/s).
691

692 ## 4. Conclusions

693 We investigated the effect of hydrodynamics and moving air-water interface (AWI)
694 on colloid retention and detachment by direct observation of colloid behavior relative to

AWI both for receding and advancing scenarios. Processes similar to the ones observed in this study can take place in unsaturated porous media, in particular, during drainage and infiltration events. The complex flow pattern observed in a trapezoidal channel here is representative of flow field in proximity of AWI in irregular soil capillaries of angular shapes. Both experimental results and theoretical analysis showed that retention of dispersed colloids at AWI is unlikely. Nevertheless, geometry and flow pattern of advancing or receding AWI may promote retention of dispersed colloids on the contact line and in angular corners of capillaries as well as allow temporary storage of colloids in the regions of residual saturation prior to infiltration events. Another contribution of dynamic AWI to colloid transport is mobilization of previously deposited or *in situ* colloids by passing fronts. Air front appears to be more efficient in mobilizing colloids as well as in serving as carrier of mobilized colloids than water front. This implies a greater potential of drainage than infiltration events in mobilizing colloids and the important role AWI can play in colloid transport in natural porous media.

The total effect of colloid transport by AWI may seem less important due to small amount of colloids retained and transported with AWI, compared to the colloid transport by the bulk flow. However, transport of colloids by AWI cannot be ignored especially when colloid deposition and straining in soil porous media are considerable and colloid remobilization by moving AWI may contribute significantly to overall colloid transport. Under these conditions, transport of colloids by AWI for considerably long distances is a possible mechanism, which should be given special attention in cases of highly toxic colloid-associated contaminants, posing a hazard in small quantities. The important

effects of dynamic AWI on colloid mobilization and transport should also be considered in modeling colloid transport under transient unsaturated conditions.

Appendix A: Solving Single-Phase Velocity Distribution in a Trapezoidal Channel

The analytical approach used to obtain the velocity distribution in a trapezoidal channel follows the method of *Shah* [1975], originally designed to analyze steady-state, fully developed laminar flow in a duct of constant cross-section area and arbitrary cross-section shape. The method is essentially a least-squares approach. Assuming constant fluid properties, the Navier-Stokes equations for steady-state, fully developed unidirectional laminar flow can be reduced to a Laplace's equation after a proper transformation using a polar coordinates system. The general solution of the Laplace's equation subject to a no-slip boundary condition on the wall surface is readily found in terms of summation of harmonic polynomials. The unknown coefficients of the polynomials are determined by a singular value decomposition algorithm because the number of boundary points typically exceeds the number of the coefficients needed to capture the nonuniform velocity distribution in the channel. In the calculations presented in Fig. 5 and Fig. A1, 60 polynomials were chosen with up to 600 boundary points used to best fit the coefficients. The results were unchanged if more terms or more boundary points were included.

The numerical method (lattice-Boltzmann or LBM) solves the lattice-Boltzmann equation for the distribution function of mesoscopic particles with a prescribed forcing field to model the driving force for the flow. The standard D3Q19 model [*Qian et al.*,

740 1992] was used with an equilibrium distribution function appropriate for incompressible
741 flow [*He and Luo*, 1997]. The macroscopic hydrodynamic variables, the fluid velocity
742 and pressure, are computed in terms of the moments of particle distribution function. The
743 no-slip boundary condition at the wall was achieved with second-order accuracy by
744 employing an interpolated bounce-back scheme. The inlet and outlet were treated with
745 periodic boundary condition in the bulk flow direction.

746 Fig. A1 provides a quantitative comparison between LBM simulation and the
747 analytical solution where the axial velocity, normalized by its maximum, on this diagonal
748 cut of the channel cross section is shown as a function of distance from the upper left
749 corner, normalized by the length of the top wall. The fact that the velocity profiles are
750 essentially identical demonstrates the accuracy of the LBM simulation and the analytical
751 solution. A significant region near the lower corners has a velocity less than 10% of the
752 maximum: 9.1% of the line length here as compared to about 5% for a simple parabolic
753 velocity profile.

754

755 **Appendix B: Simulation of Two-Phase Flow Development in a 2D Channel**

756 The simulation was carried out for a long channel where the interface is initially
757 placed at a quarter of the channel length. Fig. B1 illustrates how the flow in the channel
758 develops under the prescribed inlet and outlet conditions for both advancing and receding
759 flow scenarios.

760 It can be observed that the interface movement reaches a steady state after the time t
761 $> 2a/u$, where a is the channel width and u is the mean flow speed. During the steady
762 state, the interface establishes a dynamic contact angle, which is different from the static

763 contact angle (set to about 67°). The simulated dynamic contact angles are about 53°
764 degrees and 77° for the moving air front and for moving water front, respectively. These
765 compare well to the experimental observations and literature values of 53° and 79° for
766 the air front and the water front, respectively [*Erbil et al*., 1999; *Lim et al*., 2001;
767 *Kaczmarek and Chaberska*, 2006]. The reasonable comparison of dynamic contact angles
768 further supports the qualitative value of the simulations.
769

770 **Appendix C: Force Formulation for Equation of Colloid Motion**

771 Fig. C1 illustrates a colloid approaching AWI as well as the normal and tangential
772 directions relative to AWI [*Spielman and Goren*, 1970]. In normal direction, the drag
773 force F_D^n emerges due to the differences in colloid and fluid velocities at approach to
774 AWI and can be determined by superposition of the two cases, i.e., a moving colloid in
775 quiescent fluid and a stationary colloid in undisturbed flow normal to the AWI:
776

777 $$F_D^n = 6\pi\mu r[\frac{v_n - v_{front}\cos\alpha}{F_1} - (u_n - v_{front}\cos\alpha)F_2] \quad \text{(C1)}$$

778

779 where $(v_n - v_{front}\cos\alpha)$ and $(u_n - v_{front}\cos\alpha)$ are colloid and fluid relative velocities in
780 normal direction, respectively. F_1 and F_2 are universal hydrodynamic functions of
781 dimensionless separation H between the particle and the surface (AWI), expressed as $H = h/r$ with h as separation distance. Functions F_1 and F_2 have been obtained by *Brenner*
783 [1961] and by *Goren and O'Neill* [1971], respectively, to account for short-range
784 (viscous) hydrodynamic interactions close to a surface (wall). The expressions for F_1 and

785 F_2 generally depend on the geometry of the collector (e.g., spherical, cylindrical, etc.),
786 but can be used for any geometry if the distance between the particle and the collector is
787 sufficiently small [*Russel et al*., 1989]. F_1 can be specified as a ratio of the particle
788 velocity under an applied force (normally to the collector) to the particle velocity under
789 the same force away from the collector [*Spielman*, 1977] and F_2 as a ratio of the force
790 exerted by the flow at the particle (normal to the collector) to the force exerted on the
791 particle in an uniform flow away from the collector [*Spielman*, 1977; *Russel et al*., 1989].
792 In this study, approximate expressions for F_1 and F_2 provided by *Warszynski* [2000]
793 were used, which are expressed as:
794

795 $$F_1(H) = \frac{19H^2 + 4H}{19H^2 + 26H + 4} \qquad \text{(C2)}$$

796 and

797 $$F_2(H) = 1 + \frac{1.79}{(0.828 + H)^{1.167}}. \qquad \text{(C3)}$$

798

799 Expressions for colloid forces $F_{col} = F_{el} + F_{vdW} + F_h$ were obtained by
800 differentiating the previously used energy expressions [e.g., *Lazouskaya et al*., 2006;
801 *Lazouskaya and Jin*, 2008] as $F = -(dV / dh)$. Gravity force $\vec{F}_G$ acts in *z*-direction
802 (perpendicular to the observed in Fig. C1 area) and, therefore, is not accounted for in the
803 essentially 2D case considered in Fig. C1. Moreover, the net gravity force, calculated as
804 $F_G = (4/3)\pi r^3(\rho - \rho_f)g$, is a negligibly small value thus can be neglected for 500-nm
805 particles.

806 The force of Brownian motion has random direction and value and can be modeled
807 as a Gaussian white noise process [*Kim and Zydney*, 2004; *Johnson et al*., 2007; *Gao et*
808 *al*., 2008]. The force of Brownian motion is expressed as $F_{Br} = \delta\sqrt{12\pi\mu rkT/\Delta t}$ in each
809 spatial direction where δ denotes random numbers obeying normal distribution (with
810 zero mean and unit standard deviation) and Δt is the time step. The choice of Δt is
811 usually performed taking into account the inertial response time (or, momentum
812 relaxation time) of the colloid expressed as $\tau_p = 2\rho r^2/9\mu$ [*Kim and Zydney*, 2004; *Gao*
813 *et al*., 2008]. The time step bigger than the inertial response time is usually employed in
814 order to neglect particle inertia [*Maniero and Canu*, 2006; *Johnson et al*., 2007].
815 However, in many practical problems the time step needs to be adjusted in order to
816 account for the important, e.g., scale-related, changes in the system [*Maniero and Canu*,
817 2006; *Johnson et al*., 2007]. Also, *Gao et al*. [2008] assumed a larger response time in
818 their simulations, which was shown to have no or negligible effect on the results. In this
819 study, the time step was taken as 6.4×10^{-5} s, same as used by *Gao et al*. [2008], based on
820 the similarity of colloid properties and flow velocity in both studies.
821 Similarly, in tangential direction, there are also necessary corrections to the
822 hydrodynamic components due to the collector proximity. Universal functions F_4 and F_3
823 in tangential direction, analogous to functions F_1 and F_2 in normal direction, have been
824 computed by *Goren and O'Neill* [1971]. The correction for colloid mobility F_1 (normal)
825 is bigger than F_4 (tangential), and the wall effect is much more considerable in the
826 normal direction [*Warszynski*, 2000]. Another difference from the normal case is that
827 colloid forces do not operate in the tangential direction. Therefore, in this study we
828 limited the estimation of forces and their comparison to the normal direction.

Supporting Material

The online version of this article contains supporting video material.

Acknowledgments

This study was supported by National Research Initiative Competitive Grant no. 2006-02551 from the USDA Cooperative State Research, Education, and Extension Services.

References

Adamson, A. W., and A. P. Gast (1997), *Physical Chemistry of Surfaces*, John Wiley&Sons, New York.

Atencia, J., and D.J. Beebe (2005), Controlled microfluidic interfaces, *Nature*, *437*, 648-655, doi:10.1038/nature04163.

Auset, M., and A. A. Keller (2004), Pore-scale processes that control dispersion of colloids in saturated porous media, *Water Resour. Res.*, *40*, W03503, doi:10.1029/2003WR002800.

Auset, M., A. A. Keller, F. Brissaud, and V. Lazarova (2005), Intermittent filtration of bacteria and colloids in porous media, *Water Resour. Res.*, *41*, W09408, doi:10.1029/2004WR003611.

Baumann, T., and C. J. Werth (2004), Visualization and modeling of polystyrol colloid transport in a silicon micromodel, *Vadose Zone J.*, *3*, 434-443.

Bowen, W. R., and T. A. Doneva (2002), Atomic force microscopy of membranes, in *Encyclopedia of Surface and Colloid Science*, edited by A. T. Hubbard, pp. 664-681, Marcel Dekker, New York.

Bradford, S. A., J. Simunek, M. Bettahar, M.Th. van Genuchten, and S.R. Yates (2006), Significance of straining in colloid deposition: Evidence and implications, *Water Resour. Res.*, *42*, W12S15, doi:10.1029/2005WR004791.

Bradford, S. A., and S. Torkzaban (2008), Colloid transport and retention in unsaturated porous media: A review of interface-, collector-, and pore-scale processes and models, *Vadose Zone J.*, *7*, 667-681, doi:10.2136/vzj2007.0092.

Brenner, H. (1961), The slow motion of a sphere through a viscous fluid towards a plane surface, *Chem. Eng. Sci.*, *16*(3-4), 242-251.

Butt, H.-J., B. Cappella, and M. Kappl (2005), Force measurements with the atomic force microscope: Technique, interpretation and applications, *Surf. Sci. Rep.*, *59*, 1-152, doi:10.1016/j.surfrep.2005.08.003.

Chen, G., and M. Flury (2005), Retention of mineral colloids in unsaturated porous media as related to their surface properties, *Colloids Surf. A*, *256*, 207-216, doi:10.1016/j.colsurfa.2005.01.021.

Cheng, T., and J. E. Saiers (2008), Mobilization and transport of in-situ colloids during drainage and imbibition of partially saturated sediments, *Water Resour. Res.*, submitted.

869 Crist, J. T., J. F. McCarthy, Y. Zevi, P. Baveye, J. A. Throop, and T. S. Steenhuis (2004),
870 Pore-scale visualization of colloid transport and retention in partly saturated porous
871 media, *Vadose Zone J.*, *3*, 444-450.

872 Crist, J. T., Y. Zevi, J. F. McCarthy, J. A. Throop, and T. S. Steenhuis (2005), Transport
873 and retention mechanisms of colloids in partially saturated porous media, *Vadose Zone J.*,
874 *4*, 184-195.

875 de Gennes, P. G. (1985), Wetting: statics and dynamics, *Rev. Mod. Phys.*, *57*(3), 827-863.

876 Dussan V., E. B. (1977), Immiscible liquid displacement in a capillary tube: The moving
877 contact line, *AIChE J.*, *23*(1), 131-133.

878 Dussan V, E. B. (1979), On the spreading of liquids on solid surfaces: static and dynamic
879 contact lines, *Ann. Rev. Fluid Mech.*, *11*, 371-400.

880 El-Farhan, Y. H., N. M. Denovio, J. S. Herman, and G. M. Hornberger (2000),
881 Mobilization and transport of soil particles during infiltration experiments in an
882 agricultural field, Shenandoah Valley, Virginia, *Environ. Sci. Technol.*, *34*(17), 3555-
883 3559, doi:10.1021/es991099g.

884 Erbil, H. Y., G. McHale, S. M. Rowan, and M. I. Newton (1999), Determination of the
885 receding contact angle of sessile drops on polymer surfaces by evaporation, *Langmuir*,
886 *15*, 7378-7385, doi:10.1021/la9900831.

887 Fermigier, M., and P. Jenffer (1991), An experimental investigation of the dynamic
888 contact angle in liquid-liquid systems, *J. Colloid Interface Sci.*, *146*(1), 226-241.

889 Franzini J. B., and E. J. Finnemore (1997), *Fluid Mechanics with Engineering*
890 *Applications*, WCB/McGraw-Hill, New-York.

891 Fuentes, J., and R. L. Cerro (2007), Surface forces and inertial effects on moving contact
892 lines, *Chem. Eng. Sci.*, *62*, 3231-3241, doi:10.1016/j.ces.2007.03.012.

893 Gao, B., J. E. Saiers, and J. Ryan (2006), Pore-scale mechanisms of colloid deposition
894 and mobilization during steady and transient flow through unsaturated granular media,
895 *Water Resour. Res.*, *42*, W01410, doi:10.1029/2005WR004233.

896 Gao, H., J. Han, Y. Jin, and L.-P. Wang (2008), Modelling microscale flow and colloid
897 transport in saturated porous media, *Int. J. Comp. Fluid Dyn.*, *22*(7), 493-505,
898 doi:10.1080/10618560802238259.

899 Ginn, T. R., B. D. Wood, K. E. Nelson, T. D. Scheibe, E. M. Murphy, and T. P. Clement
900 (2002), Processes in microbial transport in the natural subsurface, *Adv. Water Resour.*,
901 *25*, 1017-1042.

902 Goldenberg, L. C., I. Hutcheon, and N. Wardlaw (1989), Experiments on transport of
903 hydrophobic particles and gas bubbles in porous media, *Transport Porous Med*., *4*, 129-
904 145.

905 Gomez Suarez C., J. Noordmans, H. C. van der Mei, and H. J. Busscher (1999a),
906 Removal of colloidal particles from quartz collector surfaces as stimulated by the passage
907 of liquid-air interfaces, *Langmuir*, *15*(15), 5123-5127, doi:10.1021/la981608c.

908 Gómez Suárez, C., J. Noordmans, H. C. van der Mei and H. J. Busscher (1999b),
909 Detachment of colloidal particles from collector surfaces with different electrostatic
910 charge and hydrophobicity by attachment to air bubbles in a parallel plate flow chamber,
911 *Phys. Chem. Chem. Phys*., *1*, 4423-4427.

912 Gómez-Suárez, C., H. J. Busscher, and H. C. van der Mei (2001a), Analysis of bacterial
913 detachment from substratum surfaces by the passage of air-liquid interfaces, *Appl.*
914 *Environ. Microbiol*., *67*(6), 2531-2537.

915 Gómez-Suárez, C., H. C. van der Mei, and H. J. Busscher (2001b), Air bubble-induced
916 detachment of polystyrene particles with different sizes from collector surfaces in a
917 parallel plate flow chamber, *Colloids Surf. A*, *186*, 211-219.

918 Goren, S. L., and M. E. O'Neill (1971), On the hydrodynamic resistance to a particle of a
919 dilute suspension when in the neighbourhood of a large obstacle, *Chem. Eng. Sci*., *26*,
920 325-338.

921 Graciaa, A., G. Morel, P. Saulner, J. Lachaise, and R. S. Schechter (1995), The ζ-
922 potential of gas bubbles, *J. Colloid Interface Sci*., *172*, 131-136.

923 Happel, J., and H. Brenner (1973), *Low Reynolds Number Hydrodynamics*, Noordhoff
924 International Publishing, Leyden.

925 He, X.Y., and Luo, L.-S. (1997), Lattice Boltzmann model for the incompressible Navier-
926 Stokes equation. *J. Stat. Phys.*, *88*(3-4), 927-944.

927 Hoek, E. M. V., S. Bhattacharjee, and M. Elimelech (2003), Effect of membrane surface
928 roughness on colloid-membrane DLVO interactions, *Langmuir*, *19*, 4836-4847,
929 doi:10.1021/la027083c.

930 Hoffman, R. L. (1975), A study of the advancing interface. I. Interface shape in liquid-
931 gas systems, *J. Colloid Interface Sci*., *50*(2), 228-241.

932 Ichikawa, N., M. Kawaji, C. Lorencez, and K. Takata (1994), Flow distribution near
933 interface of capillary flow in a tube using photochromic dye activation method,
934 *Microgravity Sci. Technol*., *7*(2), 156-159.

935 Jin, Y., and M. Flury (2002), Fate and transport of viruses in porous media, *Adv. Agron*.,
936 *77*, 39-102.

937 Johnson, D. J., N. J. Miles, and N. Hilal (2006), Quantification of particle-bubble
938 interactions using atomic force microscopy: a review, *Adv. Colloid Interface Sci*., *127*,
939 67-81, doi:10.1016/j.cis.2006.11.005.

940 Johnson, W. P., X. Li, and G. Yal (2007), Colloid retention in porous media: Mechanistic
941 confirmation of wedging and retention in zones of flow stagnation, *Environ. Sci.*
942 *Technol*., *41*(4), 1279-1287, doi:10.1021/es061301x.

943 Kaczmarek, H., and H. Chaberska (2006), The influence of UV-irradiation and support
944 type on surface properties of poly(methyl methacrylate) thin films, *Appl. Surf. Sci*., *252*,
945 8185-8192, doi:10.1016/j.apsusc.2005.10.037.

946 Kalliadasis, S., and H.-C. Chang (1994), Apparent dynamic contact angle of an
947 advancing gas-liquid meniscus, *Phys. Fluids*, *6*(1), 12-23.

948 Kang, Q., D. Zhang, and S. Chen (2004), Immiscible displacement in a channel:
949 simulations of fingering in two dimensions. *Adv. Water Res*., *27*, 13-22,
950 doi:10.1016/j.advwatres.2003.10.002.

951 Karnis, A., and S. G. Mason (1967), The flow of suspensions through tubes. VI.
952 Meniscus effects, *J. Colloid Interface Sci*., *23*, 120-133.

953 Kim, M., and A. L. Zydney (2004), Effect of electrostatic, hydrodynamic, and Brownian
954 forces on particle trajectories and sieving in normal flow filtration, *J. Colloid Interface*
955 *Sci*., *269*, 425-431, doi:10.1016/j.jcis.2003.08.004.

956 Kinoshita, H., S. Kaneda, T. Fujii, and M. Oshima (2007), Three-dimensional
957 measurement and visualization of internal flow of a moving droplet using confocal
958 micro-PIV, *Lab Chip*, *7*, 338-346.

959 Kolb, W. B., and R. L. Cerro (1993), The motion of long bubbles in tubes of square cross
960 section, *Phys. Fluids A*, *5*(7), 1549-1557.

961 Kuznar, Z. A., and M. Elimelech (2007), Direct microscopic observation of particle
962 deposition in porous media: Role of the secondary energy minimum, *Colloids Surf. A*,
963 *294*, 156-162, doi:10.1016/j.colsurfa.2006.08.007.

964 Lazouskaya, V., Y. Jin, and D. Or (2006), Interfacial interactions and colloid retention
965 under steady flows in a capillary channel, *J. Colloid Interface Sci*., *303*, 171-184,
966 doi:10.1016/j.jcis.2006.07.071.

967 Lazouskaya, V., and Y. Jin (2008), Colloid retention at air-water interface in a capillary
968 channel, *Colloids Surf. A*, *325*, 141-151, doi:10.1016/j.colsurfa.2008.04.053.

969 Lecoanet, H. F., J.-Y. Bottero, and M. R. Wiesner (2004), Laboratory assessment of the
970 mobility of nanomaterials in porous media, *Environ. Sci. Technol*., *38*(19), 5164-5169,
971 doi:10.1021/es0352303.

Leenaars, A. F. M. (1988), A new approach to the removal of sub-micron particles from solid (silicon) substrates, in *Particles on Surfaces 1: Detection, Adhesion, and Removal*, edited by K. L. Mittal, pp. 361-372, Plenum Press, New York.

Leenaars, A. F. M., and S. B. G. O'Brien (1989), Particle removal from silicon substrates using surface tension forces, *Philips J. Res*., *44*, 183-209.

Lim, H., Y. Lee, S. Han, J. Cho, and K.-J. Kim (2001), Surface treatment and characterization of PMMA, PHEMA, and PHPMA, *J. Vac. Sci. Technol. A*, *19*(4), 1490-1496.

Lubeck, C. R., M. C. Chin, and F. M. Doyle (2003), Functionalization of a synthetic polymer to create inorganic/polymer hybrid materials, in *Functional Fillers and Nanoscale Minerals*, edited by J. J. Kellar, M. A. Herpfer, and B. M. Moudgil, pp. 95-104, SME, Littleton.

Maniero, R., and P. Canu (2006), A model of fine particles deposition on smooth surfaces: I-Theoretical basis and model development, *Chem. Eng. Sci*., *61*, 7626-7635, doi:10.1016/j.ces.2006.08.064.

McCarthy, J. F., and J. M. Zachara (1989), Subsurface transport of contaminants, *Environ. Sci. Technol*., *23*(5), 496-502.

Mumley, T. E., C. J. Radke, and M. C. Williams (1986a), Kinetics of liquid/liquid capillary rise. I. Experimental observations, *J. Colloid Interface Sci*., *109*(2), 398-412.

Mumley, T. E., C. J. Radke, and M. C. Williams (1986b), Kinetics of liquid/liquid capillary rise. II. Development and test of theory, *J. Colloid Interface Sci*., *109*(2), 413-425.

Nalaskowski, J., A. V. Nguyen, J. Hupka, and J. D. Miller (2002), Study of particle-bubble interaction using atomic force microscopy – current possibilities and challenges, *Physicochem. Probl. Miner. Process*., *36*, 253-272.

Nguyen, A. V., and H. J. Schulze (2004), *Colloidal Science of Flotation*, Marcel Dekker, New York.

Noordmans, J., P. J. Wit, H. C. van der Mei, and H. J. Busscher (1997), Detachment of polystyrene particles from collector surfaces by surface tension forces induced by air-bubble passage through a parallel plate flow chamber, *J. Adhesion Sci. Technol*., *11*(7), 957-969.

Ochiai, N., E. L. Kraft, and J. S. Selker (2006), Methods for colloid transport visualization in pore networks, *Water Resour. Res*., *42*, W12S06, doi:10.1029/2006WR004961.

1006 Petkov, J. T., and N. D. Denkov (2002), Dynamics of particles at interfaces and in thin
1007 liquid films, in *Encyclopedia of Surface and Colloid Science*, edited by A. T. Hubbard,
1008 pp. 1529-1545, Marcel Dekker, New York.

1009 Pismen, L. M. (2002), Mesoscopic hydrodynamics of contact line motion, *Colloids Surf.*
1010 *A*, *206*, 11-30.

1011 Pnueli, D., and C. Gutfinger (1992), *Fluid Mechanics*, Cambridge University Press,
1012 Cambridge.

1013 Pomeau, Y. (2002), Recent progress in the moving contact line problem: a review, *C. R.*
1014 *Mecanique*, *330*, 207-222.

1015 Qian, Y. H., D. d'Humières, and P. Lallemand (1992), Lattice BGK models for Navier-
1016 Stokes equation. *Europhys. Lett.*, *17*(6), 479-484.

1017 Roizard, C., S. Poncin, F. Lapicque, X. Py, and N. Midoux (1999), Behavior of fine
1018 particles in the vicinity of a gas bubble in a stagnant and moving fluid, *Chem. Eng. Sci*.,
1019 *54*, 2317-2323.

1020 Ross, S., and I. D. Morrison (1989), *Colloidal Systems and Interfaces*, John Wiley &
1021 Sons, New York.

1022 Russel, W. B., D. A. Saville, and W. R. Schowalter (1989), *Colloidal Dispersions*,
1023 Cambridge University Press, Cambridge.

1024 Saiers, J. E., G. M. Hornberger, D. B. Gower, and J. S. Herman (2003), The role of
1025 moving air-water interfaces in colloid mobilization within the vadose zone, *Geophys.*
1026 *Res. Lett*., *30*(21), 2083, doi:10.1029/2003GL018418.

1027 Saiers, J. E., and J. N. Ryan (2006), Introduction to special section on Colloid Transport
1028 in Subsurface Environments, *Water Resour. Res*., *42*, W12S01,
1029 doi:10.1029/2006WR005620.

1030 Schulze, H. J. (1984), *Physico-chemical Elementary Processes in Flotation*, Elsevier,
1031 Amsterdam.

1032 Sen, T. K., and K. C. Khilar (2006), Review on subsurface colloids and colloid-
1033 associated contaminant transport in saturated porous media, *Adv. Colloid Interface Sci*.,
1034 *119*, 71-96, doi:10.1016/j.cis.2005.09.001.

1035 Shah, P. K. (1975), Laminar flow friction and forced convection heat transfer in ducts of
1036 arbitrary geometry, *Int. J. Heat Mass Transfer*, *18*, 849-862.

1037 Shang, J., M. Flury, G. Chen, and J. Zhuang (2008), Impact of flow rate, water content,
1038 and capillary forces on in situ colloid mobilization during infiltration in unsaturated
1039 sediments, *Water Resour. Res*., *44*, W06411, doi:10.1029/2007WR006516.

1040 Sharma, P., H. M. Abdou, and M. Flury (2008a), Effect of the lower boundary condition
1041 and flotation on colloid mobilization in unsaturated sandy sediments, *Vadose Zone J.*, *7*,
1042 930-940, doi:10.2136/vzj2007.0163.

1043 Sharma, P., M. Flury, and J. Zhou (2008b), Detachment of colloids from a solid by a
1044 moving air-water interface, *J. Colloid Interface Sci*., *326*(1), 143-150,
1045 doi:10.1016/j.jcis.2008.07.030.

1046 Shikhmurzaev, Y. D. (2006), Singularities at the moving contact line. Mathematical,
1047 physical and computational aspects, *Physica D*, *217*, 121-133,
1048 doi:10.1016/j.physd.2006.03.003.

1049 Sirivithayapakorn, S., and A. Keller (2003a), Transport of colloids in saturated porous
1050 media: A pore-scale observation of the size exclusion effect and colloid acceleration,
1051 *Water Resour. Res*., *39*(4), 1109, doi:10.1029/2002WR001583.

1052 Sirivithayapakorn, S., and A. Keller (2003b), Transport of colloids in unsaturated porous
1053 media: A pore-scale observation of processes during the dissolution of air-water
1054 interface, *Water Resour. Res*., *39*(12), 1346, doi:10.1029/2003WR002487.

1055 Sjollema, J., and H. J. Busscher (1989), Deposition of polystyrene latex particles toward
1056 polymethylmethacrylate in a parallel plate flow cell, *J. Colloid Interface Sci*., *132*(2),
1057 382-394.

1058 Spielman, L. A., and S. L. Goren (1970), Capture of small particles by London forces
1059 from low-speed liquid flows, *Environ. Sci. Technol*., *4*(2), 135-140.

1060 Spielman, L. A. (1977), Particle capture from low-speed laminar flows, *Ann. Rev. Fluid*
1061 *Mech*., *9*, 297-319.

1062 Suresh, L., and J. Y. Walz (1996), Effect of surface roughness on the interaction energy
1063 between a colloidal sphere and flat plate, *J. Colloid Interface Sci*., *183*, 199-213.

1064 Tanner, L. H. (1979), The spreading of silicone oil drops on horizontal surfaces, *J. Phys.*
1065 *D: Appl. Phys*., *12*, 1473-1484.

1066 Torkzaban, S., S. A. Bradford, and S. L. Walker (2007), Resolving the coupled effects of
1067 hydrodynamics and DLVO forces on colloid attachment in porous media, *Langmuir*,
1068 *23*(19), 9652-9660, doi:10.1021/la700995e.

1069 Torkzaban, S., S. A. Bradford, M. Th. van Genuchten, and S. L. Walker (2008a), Colloid
1070 transport in unsaturated porous media: The role of water content and ionic strength on
1071 particle straining, *J. Contam. Hydrol*., *96*, 113-127, doi:10.1016/j.jconhyd.2007.10.006.

1072 Torkzaban, S., S. S. Tazehkand, S. L. Walker, and S. A. Bradford (2008b), Transport and
1073 fate of bacteria in porous media: Coupled effects of chemical conditions and pore space
1074 geometry, *Water Resour. Res*., *44*, W04403, doi:10.1029/2007WR006541.

van Remoortere, P., and P. Joos (1991), The kinetics of wetting: the motion of a three phase contact line in a capillary, *J. Colloid Interface Sci*., *141*(2), 348-359.

Wan, J., and J. L. Wilson (1992), Colloid transport and the gas-water interface in porous media, in *Transport and Remediation of Subsurface Contaminants: Colloidal, Interfacial, and Surfactant Phenomena*, edited by D. A. Sabatini and R. C. Knox, pp. 55-70, American Chemical Society, Washington, DC.

Wan, J., and J. L. Wilson (1993), Visualization of colloid transport during single and two-fluid flow in porous media, in: *Manipulation of Groundwater Colloids for Environmental Restoration*, edited by J. F. McCarthy and F. J. Wobber, pp. 335-339, CRC Press, Boca Raton.

Wan, J., and J. L. Wilson (1994), Visualization of the role of the gas-water interface on the fate and transport of colloids in porous media, *Water Resour. Res*., *30*(1), 11-23.

Wan, J., J. L. Wilson, and T. L. Kieft (1994), Influence of the gas-water interface on transport of microorganisms through unsaturated porous media, *Appl. Environ. Microbiol*., *60*(2), 509-516.

Warszynski, P. (2000), Coupling of hydrodynamic and electric interactions in adsorption of colloidal particles, *Adv. Colloid Interface Sci*., *84*, 47-142.

Wiesner, M. R., G. V. Lowry, P. Alvarez, D. Dionysiou, and P. Bismas (2006), Assessing the risks of manufactured nanomaterials, *Environ. Sci. Technol*., *40*(14), 4336-4345.

Yao K.-M., M. T. Habibian, and C. R. O'Melia (1971), Water and waste water filtration: Concepts and applications, *Environ. Sci. Technol*., *5*(11), 1105-1112.

Yuan, P, and L. Schaefer (2006), Equation of state in a lattice Boltzmann model, *Phys. Fluids*, *18*, 042101.

Zevi, Y., A. Dathe, J. F. McCarthy, B. K. Richards, and T. S. Steenhuis (2005), Distribution of colloid particles onto interfaces in partially saturated sand, *Environ. Sci. Technol*., *39*(18), 7055-7064, doi:10.1021/es048595b.

Zhuang, J., J. F. McCarthy, J. S. Tyner, E. Perfect, and M. Flury (2007), In situ colloid mobilization in Hanford sediments under unsaturated transient flow conditions: Effect of irrigation pattern, *Environ. Sci. Technol*., *41*(9), 3199-3204, doi:10.1021/es062757h.

Figure captions

Figure 1. Images of the microfluidic channel acquired with confocal microscope and accompanied with the schematic cross section in two regimes: (A) water front and (B) air front. In the images, the dashed lines mark the approximate location of the schematic cross sections shown on the right, and the black arrows indicate the flow direction. Note: *z*- cross section is not shown to scale.

Figure 2. Schematic flow patterns inferred from observing colloid motion relative to the front (AWI) shown for (A) water and (B) air fronts. White arrows represent direction of colloid movement relative to AWI; black arrows indicate the direction of flow and front movement.

Figure 3. Colloid approach (impact) velocities (squares) plotted against the water front velocity (line).

Figure 4. Trajectories of a colloid in the bulk flow (or 400 μm from AWI, shown with light-colored arrows) and of two colloids after interaction with the air front (shown with dark-colored arrows). The two colloids interacting with AWI were initially observed at the distance of ~ 70 – 85 μm from AWI. The trajectories are shown for the case of air front, which was moving in the direction from right to left at the velocity of 12.1 μm/s.

Figure 5. Contour of axial velocity from analytical solution, normalized by the maximum axial velocity in the cross section of the trapezoidal channel.

Figure 6. Velocity vector field relative to the moving interface for (A) water front and (B) air front, simulated for a 2D channel and analogous to the cases in Fig. 2.

Figure 7. Confocal image showing observed colloid locations in respect to the air front (left) and schematic cross section showing possible positions of colloids in the corner region (right).

Figure 8. The magnitudes of forces acting on a colloid plotted against the dimensionless separation from AWI. Note: for magnitude comparison, the direction of Brownian motion force has not been accounted for in the graph.

Figure 9. Forces acting on a particle interacting with: (A) air front ($\varphi = 53°$, receding contact angle), (B) air front, illustrated with a possible mechanism of colloid detachment, and (C) water front ($\varphi = 79°$, advancing contact angle). The horizontal arrow in the top part of the figure indicates the direction of AWI movement.

Figure A1. Comparison of steady-state, axial velocity profiles from LBM and analytical solution along the diagonal cut from the upper-left corner to the lower-right corner through the cross section of the trapezoidal channel.

Figure B1. The simulated moving interface at different times at a time interval of $0.26a/u$, where a is the channel width and u is the mean flow speed.

Figure C1. Geometry of a colloid approaching AWI.

1144 Table 1. Experimental and literature values of parameters used in calculations.

Parameter	Symbol	Value	Source
Temperature	T	298 K (25°C)	measured
Fluid density (water)	ρ_f	997 kg/m^3	Pnueli and Gutfinger, 1992
Surface tension (water)	σ	7.2×10^{-2} N/m	Adamson and Gast, 1997
Viscosity (water)	μ	8.94×10^{-4} Pa·s	Pnueli and Gutfinger, 1992
Ionic strength (DI water)	i	1.5×10^{-6} M	measured
AWI zeta-potential	ψ_{AWI}	-6.5×10^{-2} V	Graciaa et al., 1995
Colloid zeta-potential	ψ	-6.56×10^{-2} V	determined experimentally
PMMA zeta-potential	ψ_{PMMA}	-2.5×10^{-2} V	Lubeck et al., 2003
Colloid radius	r	2.5×10^{-7} m	manufacturer, determined experimentally
Colloid density	ρ	1055 kg/m^3	manufacturer
Colloid contact angle	θ	~20°	assumed based on value measured for 1.1 μm colloids (Lazouskaya et al., 2006)
Colloid velocity (typical value)	v	~10^{-5} m/s	determined experimentally
Front velocity (typical value)	v_{front}	~10^{-5} m/s	determined experimentally
Fluid velocity	v_f	~10^{-5} m/s	determined experimentally
Angle of impact	α	0 - 41°	determined experimentally
Characteristic length (channel dimension)	a	2×10^{-5} m (min) to 7×10^{-5} m (max)	manufacturer
PMMA-water contact angles: static receding advancing	φ	 72° 53° 79°	Erbil et al., 1999; Lim et al., 2001; Kaczmarek and Chaberska, 2006

1145

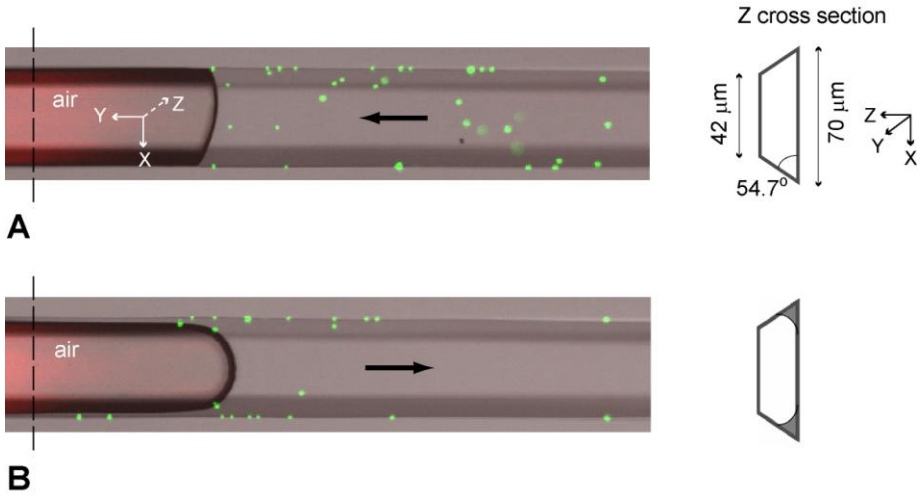

Figure .1. Images of the microfluidic channel acquired with confocal microscope and accompanied with the schematic cross section in two regimes: (A) water front and (B) air front. In the images, the dashed lines mark the approximate location of the schematic cross sections shown on the right, and the black arrows indicate the flow direction. Note: *z*- cross section is not shown to scale.

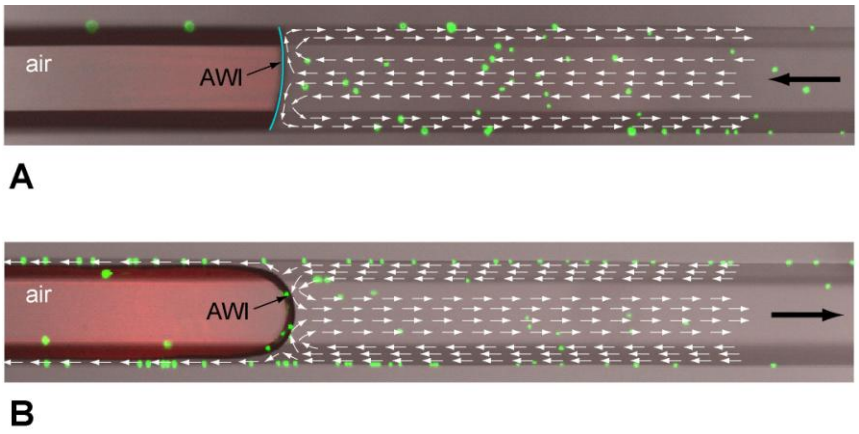

Figure 2. Schematic flow patterns inferred from observing colloid motion relative to the front (AWI) shown for (A) water and (B) air fronts. White arrows represent direction of colloid movement relative to AWI; black arrows indicate the direction of flow and front movement.

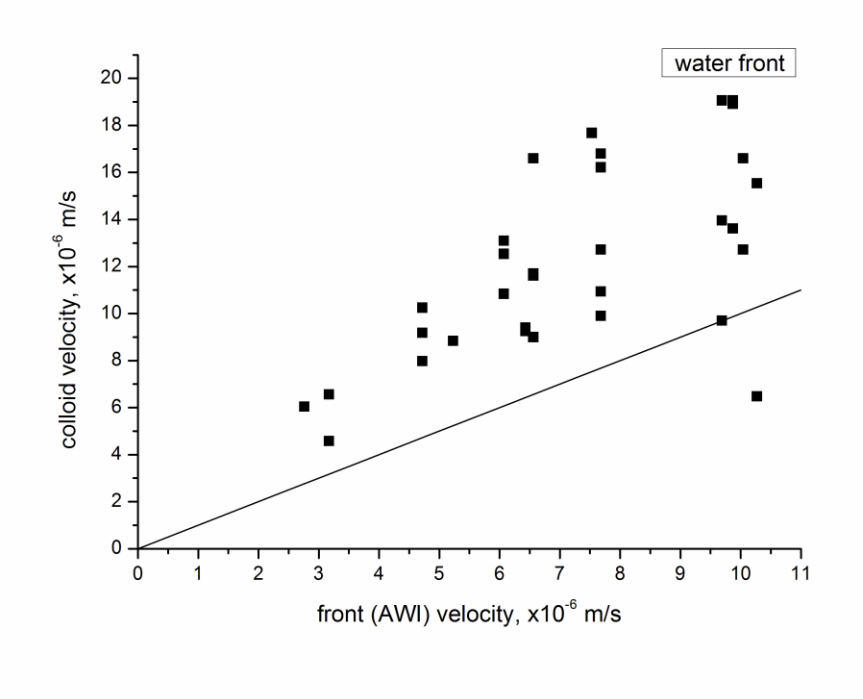

Figure 3. Colloid approach (impact) velocities (squares) plotted against the water front velocity (line).

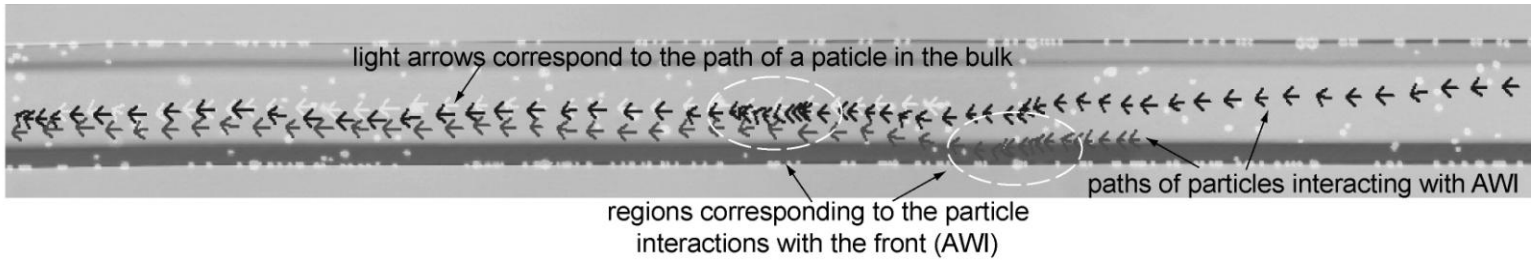

Figure 4. Trajectories of a colloid in the bulk flow (or 400 μm from AWI, shown with light-colored arrows) and of two colloids after interaction with the air front (shown with dark-colored arrows). The two colloids interacting with AWI were initially observed at the distance of ~ 70 – 85 μm from AWI. The trajectories are shown for the case of air front, which was moving in the direction from right to left at the velocity of 12.1 μm/s.

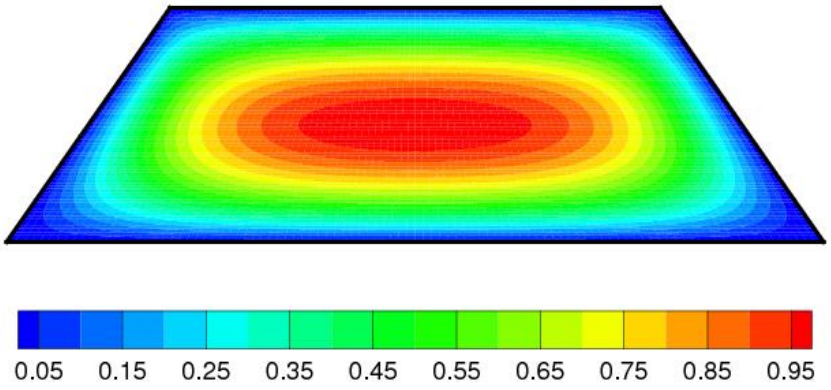

Figure 5. Contour of axial velocity from analytical solution, normalized by the maximum axial velocity in the cross section of the trapezoidal channel.

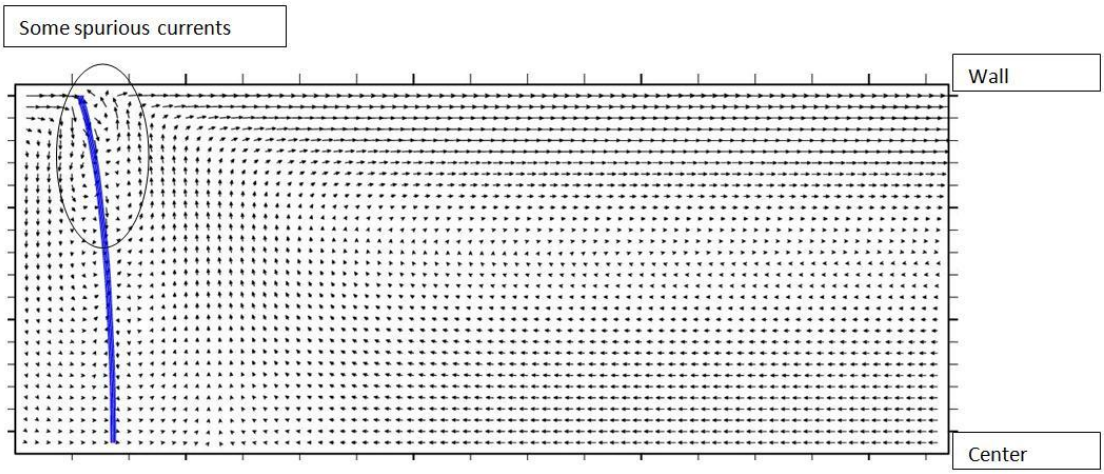

A

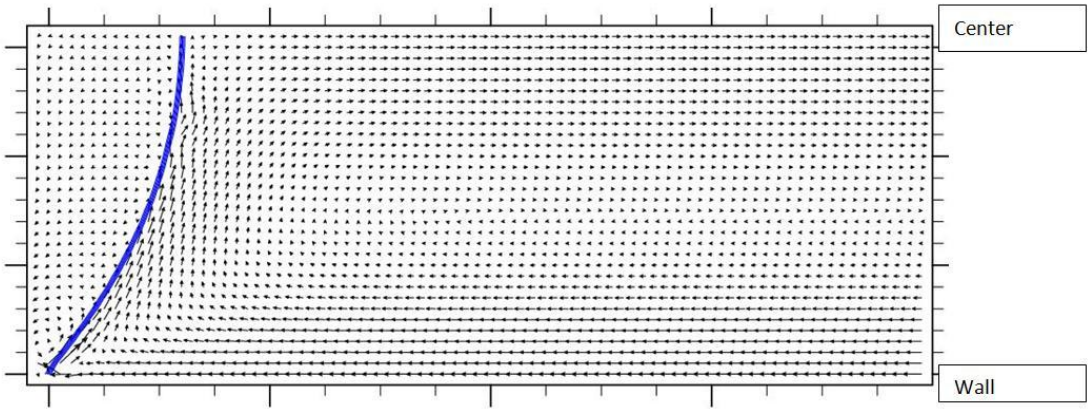

B

Figure 6. Velocity vector field relative to the moving interface for (A) water front and (B) air front, simulated for a 2D channel and analogous to the cases in Fig. 2.

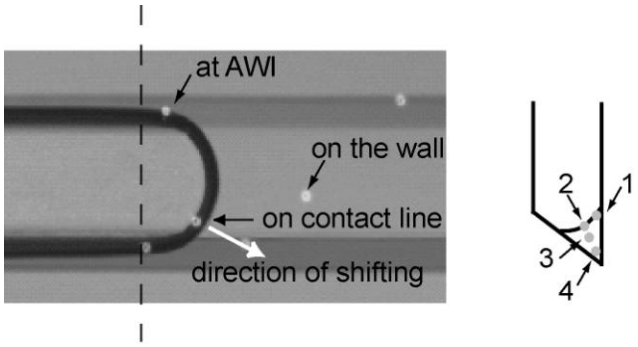

Figure 7. Confocal image showing observed colloid locations in respect to the air front (left) and schematic cross section showing possible positions of colloids in the corner region (right).

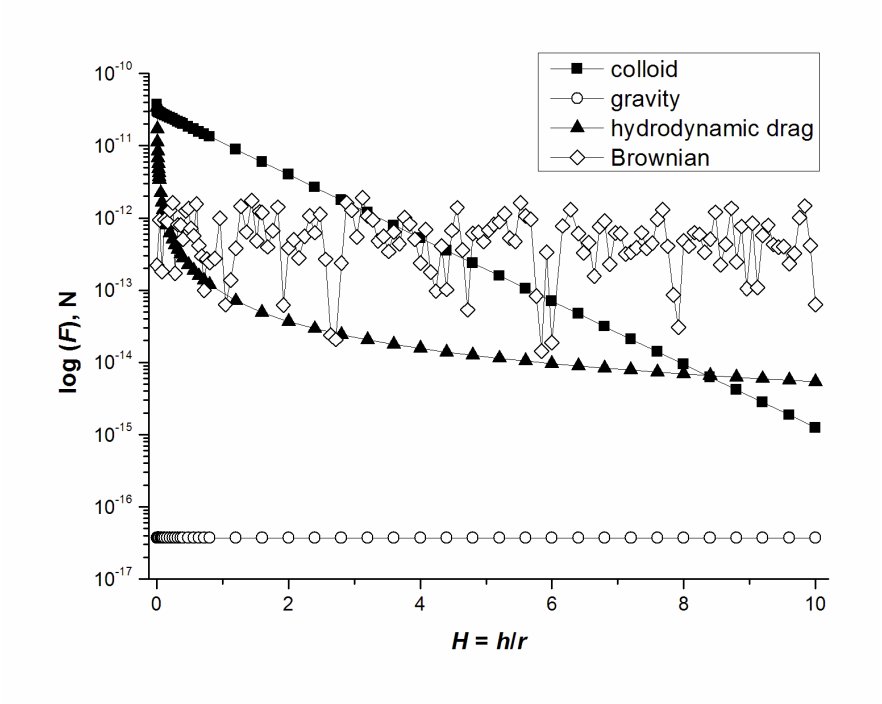

Figure 8. The magnitudes of forces acting on a colloid plotted against the dimensionless separation from AWI. Note: for magnitude comparison, the direction of Brownian motion force has not been accounted for in the graph.

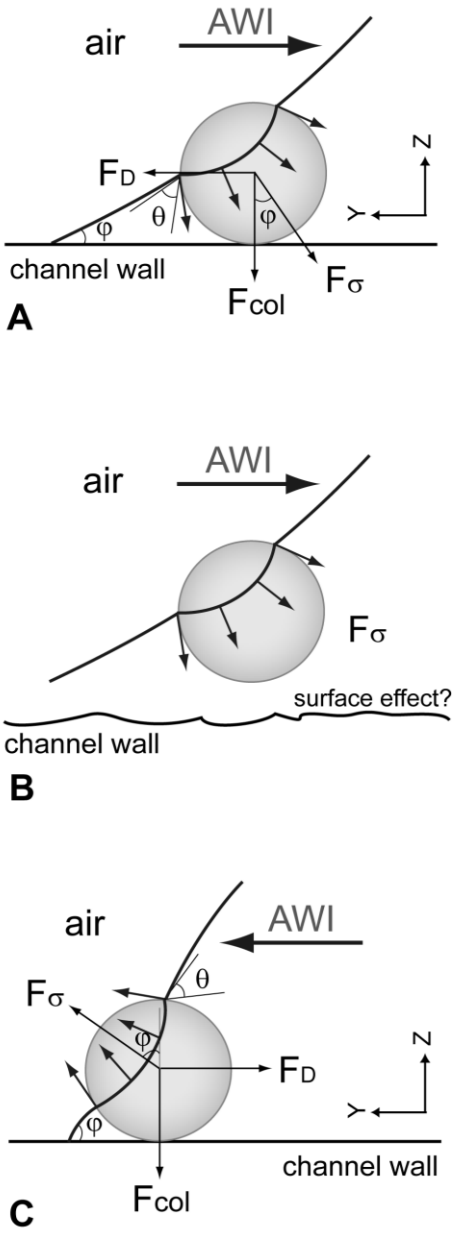

Figure 9. Forces acting on a particle interacting with: (A) air front (φ = 53°, receding contact angle), (B) air front, illustrated with a possible mechanism of colloid detachment, and (C) water front (φ = 79°, advancing contact angle). The horizontal arrow in the top part of the figure indicates the direction of AWI movement.

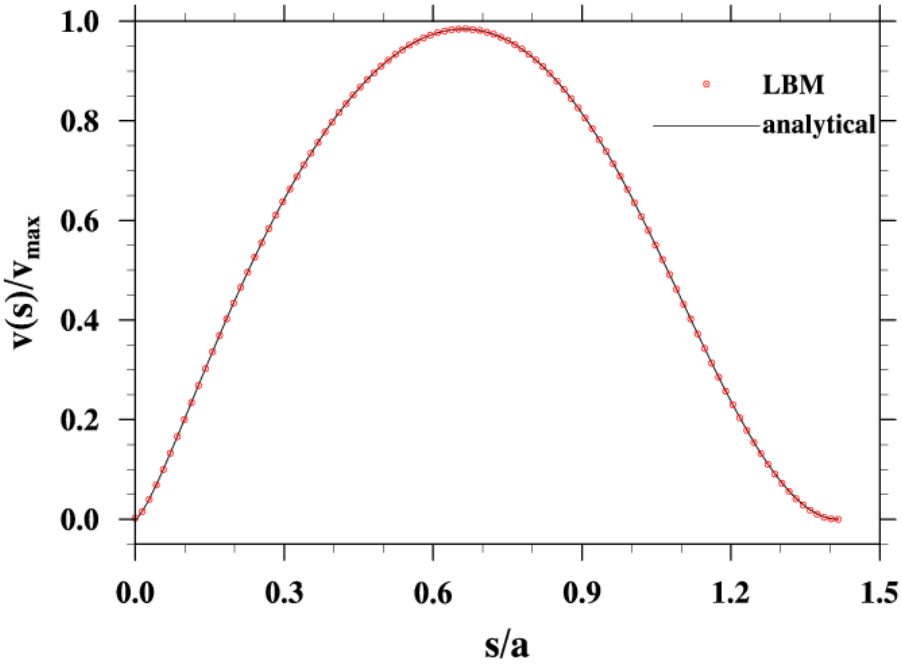

Figure A1. Comparison of steady-state, axial velocity profiles from LBM and analytical solution along the diagonal cut from the upper-left corner to the lower-right corner through the cross section of the trapezoidal channel.

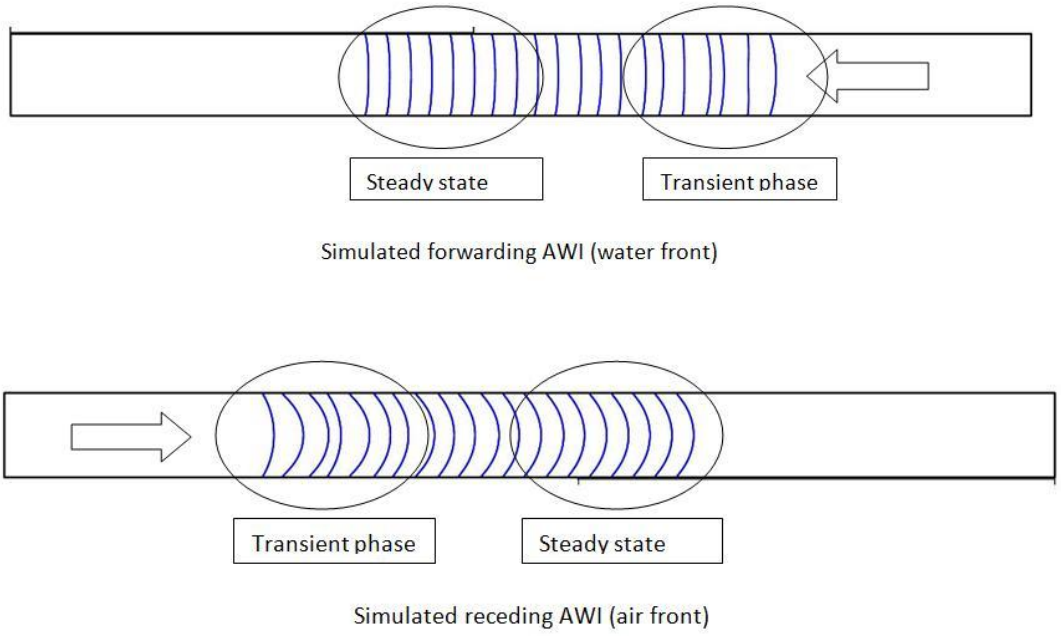

Figure B1. The simulated moving interface at different times at a time interval of $0.26a/u$, where a is the channel width and u is the mean flow speed.

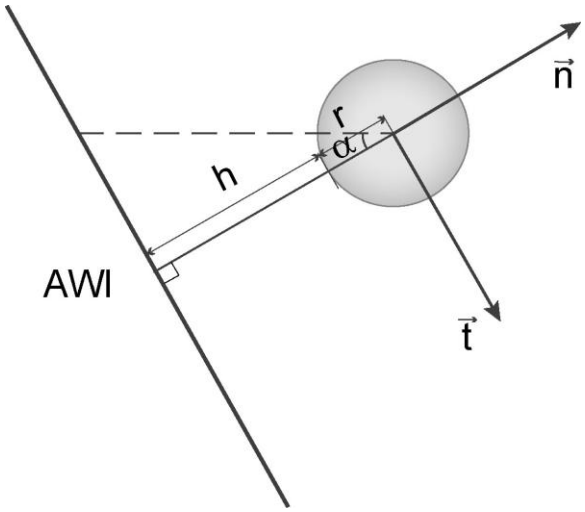

Figure C1. Geometry of a colloid approaching AWI.